MiniMax-Remover: Taming Bad Noise Helps Video Object Removal

Bojia Zi[1,6,*], **Weixuan Peng**[2,*], **Xianbiao Qi**[3,†], **Jianan Wang**[4],
Shihao Zhao[5], **Rong Xiao**[3], **Kam-Fai Wong**[1,6]

[1]The Chinese University of Hong Kong [2]Shenzhen University [3]IntelliFusion Inc.
[4]Astribot Inc. [5]The University of Hong Kong
[6]MoE Key Laboratory of High Confidence Software Technologies, CUHK

Figure 1: Visual Results of MiniMax-Remover. The left side displays the original videos, while the right side shows the edited results. Our method achieves high-quality removal of the target objects: the girl, chameleon, bird, lane line, and red wine glass, as illustrated in the five corresponding video examples. *Best viewed with Acrobat Reader. Click the images to play the animations.*

Abstract

Recent advances in video diffusion models have driven rapid progress in video editing techniques. However, video object removal, a critical subtask of video editing, remains challenging due to issues such as hallucinated objects and visual artifacts. Furthermore, existing methods often rely on computationally expensive sampling procedures and classifier-free guidance (CFG), resulting in slow inference. To address these limitations, we propose **MiniMax-Remover**, a novel two-stage

* Equal Contribution.
† Corresponding author. Email: qixianbiao@gmail.com

39th Conference on Neural Information Processing Systems (NeurIPS 2025).

video object removal approach. Motivated by the observation that text condition is not best suited for this task, we simplify the pretrained video generation model by removing textual input and cross-attention layers. In this way, we obtain a more lightweight and efficient model architecture in the first stage. In the second stage, we proposed a minimax optimization strategy to further distill the remover with the successful videos produced by stage-1 model. Specifically, the inner maximization identifies adversarial input noise ("bad noise") that leads to failure removals, while the outer minimization trains the model to generate high-quality removal results even under such challenging conditions. As a result, our method achieves a state-of-the-art video object removal results using as few as 6 sampling steps without CFG usage. Extensive experiments demonstrate the effectiveness and superiority of MiniMax-Remover compared to existing methods. Codes and Videos are available at: `https://minimax-remover.github.io`.

1 Introduction

In recent years, diffusion models [4, 3, 16, 8, 11, 37, 51, 22, 34, 33, 44, 57] have driven remarkable progress in image and video generation. UNet-based architectures, exemplified by models such as AnimateDiff [16] and VideoCrafter2 [8], have demonstrated impressive capabilities in generating high-quality videos. More recently, the field has advanced with the introduction of transformer-based architectures, as seen in groundbreaking works such as Sora [37], HunyuanVideo [22] and Wan2.1 [44], which employ DiT-based structures [38] to achieve unprecedented generation quality. Parallel to these advancements, diffusion-based editing techniques [6, 52, 47, 12, 30, 48, 2, 20, 58, 28, 49, 13, 10, 23] have also seen significant progress. Among these, *video inpainting* has emerged as a particularly crucial capability, serving as a foundational component for numerous fine-grained video editing applications.

Video object removal focuses on erasing specified objects from videos while preserving background consistency and temporal coherence. ProPainter [56] addressed this by completing optical flow within masked regions and then synthesizing the fill-in content using vision transformers, rather than relying on generative models. More recently, the field has shifted toward diffusion-based methods, with several notable advancements. FFF-VDI [24] uses optical flow and generative model to inpaint videos. DiffuEraser [25] employs DDIM inversion and vision priors to enhance video inpainting quality. Similarly, FloED [15] proposes a dual-branch architecture and a two-stage training strategy to achieve higher fidelity in the regions where objects are intended to be removed.

Despite rapid progress, existing video object removal methods still face multiple challenges. Some methods generate undesired content or artifacts, while others introduce occlusions and blurs within masked regions. Furthermore, most approaches rely heavily on auxiliary priors (*e.g.*, optical flow, text prompts, or DDIM inversion). The complicated model design lead to unsuitability and limit user-friendliness. Moreover, the generative methods require a large number of sampling steps to achieve high visual fidelity and depend on classifier-free guidance (CFG), which requires two model evaluations per sampling step, further exacerbates inference latency, limiting their practicality in real-world applications.

To address these limitations, we propose a two-stage framework for video object removal that simultaneously enhances visual quality and reduces inference cost. In **Stage 1**, we train upon Wan2.1-1.3B [44] and introduce two key modifications: (i) replacing external text prompts with learnable *contrastive condition tokens*, and (ii) removing all cross-attention layers within the DiT blocks, instead injecting contrastive condition tokens directly into the self-attention stream to enable conditional control. This lightweight conditioning approach significantly reduces computational overhead while preserving the structural integrity of the DiT backbone, allowing the same weights to be reused in the next stage, even when conditional control is disabled. In **Stage 2**, we distill the remover on manually curate 10K high-quality object removal samples generated by the model in Stage 1 and introduce a *minimax* optimization strategy to further improve object removal performance. The inner maximization searches for adversarial noise ("bad" noise) that induces model failure, while the outer minimization trains the model to be robust against such challenging cases. This minmax optimization enables our remover to consistently produce artifact-free results and prevents generating undesired objects without the assistance of CFG. As a result, the final model achieves both superior visual quality and remarkable inference efficiency compared to existing methods.

Table 1: Comparison of our MiniMax-Remover and other Video Inpainting Methods. We compare these methods on a video with 33 frames and 360P resolution on A800 GPUs, using their default configuration. "-" means unknown, while "N/A" means not applicable. Senorita-R means Senorita-2M remover expert. DiffuEraser uses ProPainter to generate prior (1 step) and PCM [45] to refine the edited output (2 steps). The motion adapter (20 steps) and DDIM inversion in DiffuEraser are both optional.

Method	Params	**•Inference Details**				**•Additional Condition / Prior**				**Open-Source**
		Min Steps	CFG	Latency (s)	GPU Mem (GB)	DDIM Inversion	Optical Flow	Text Prompt	First Frame	
AVID [55]	1.95B	-	✓	-	-	×	×	✓	×	×
FFF-VDI [24]	-	50	✓	-	-	✓	✓	×	×	×
VIVID [20]	5.57B	50	✓	-	-	×	×	✓	✓	×
Senorita-R [58]	1.69B	50	✓	-	-	×	×	✓	×	×
MTV-Inpaint [50]	1.41B	30	✓	-	-	×	×	✓	×	×
Propainter [56]	39.4M	N/A	N/A	0.20	12.1	×	✓	×	×	✓
VideoComposer [48]	1.40B	50	✓	2.83	49.1	×	×	✓	×	✓
COCOCO [59]	1.55B	50	✓	3.56	36.5	×	×	✓	×	✓
FloED [15]	1.41B	25	✓	1.32	47.6	×	✓	✓	✓	✓
DiffuEraser [25]	2.19B	3	✓	0.35	10.4	✓	×	✓	×	✓
VideoPainter [2]	5.92B	50	✓	8.14	44.7	×	×	✓	✓	✓
VACE [21]	1.78B	25	✓	1.93	23.6	×	×	✓	×	✓
MiniMax-Remover	1.12B	6	×	0.18	8.2	×	×	×	×	✓

Our main contributions are summarized as follows:

1. we propose a lightweight yet effective DiT-based architecture for video object removal. Motivated by the observation that text prompting is not best suited for the task of object removal, we replace the text conditions with learnable contrastive tokens to control the removal process. These tokens are integrated directly into the self-attention stream, allowing us to remove all cross-attention layers within the pretrained video generation model. *As a result, in Stage 1, our model features fewer parameters and no longer depends on ambiguous text instruction.*
2. In Stage 2, we distilled a remover on 10K manually selected video removals produced by the model in Stage 1, with minmax optimization strategy. Specifically, the inner maximization optimization finds a bad input noise that makes model fail, while the outer minimization optimization tries to teach model remove the bad noise added on the successful videos.
3. We conduct extensive experiments across multiple benchmarks, demonstrating that our method achieves superior performance in both inference speed and visual fidelity. As shown in Figure 4 and Table 1, *our model produces high-quality removal results using as few as 6 sampling steps and without relying on classifier-free guidance (CFG).*

2 Related Work

Video diffusion models have witnessed remarkable progress in recent years [48, 46, 16, 8, 37, 51, 33, 22, 17, 53, 44], accompanied by the emergence of various video editing techniques [27, 49, 54, 26, 35, 10, 13, 23, 9, 58]. Among these techniques, video inpainting plays a crucial role by enabling the regeneration of content in corrupted or missing regions [48, 59, 2, 21, 50, 58, 20, 55, 56, 15, 25, 58, 24]. Generally, video inpainting tasks can be categorized into two main types: one focuses on generating or editing objects within specified regions with prompts, while the other aims to remove objects based on provided masks.

Text-guided Video Inpainting. For the first type of video inpainting, which involves generating or editing content within a masked region, significant progress has been made in recent years. VideoComposer [48] is the first diffusion model capable of performing text-guided video inpainting. It supports multiple conditioning inputs and can handle various tasks within a unified framework. AVID [55] proposed a method for text-guided video inpainting of arbitrary-length sequences using natural language prompts. COCOCO [59] improves consistency and controllability through damped global attention and enhanced cross-attention to text. VIVID [20] introduces a large-scale dataset with 10M image and video samples for localized editing, enabling training of a powerful text-guided inpainter. MTV-Inpaint [50] is capable of handling both traditional scene completion and novel object insertion. VideoPainter [2] performs inpainting using a DiT-based architecture, incorporating

an efficient context encoder to process masked inputs and injecting backbone-aware background information into a pre-trained video DiT for plug-and-play consistent video inpainting.

Video Object Removal. In contrast to text-guided inpainting, some methods focus specifically on removing objects from videos. ProPainter [56] uses optical flow to first complete the motion in masked regions, then synthesizes inpainted content accordingly. FFF-VDI [24] propagates noise latents from future frames to fill masked areas in the initial latent space, then finetunes a pre-trained image-to-video diffusion model for final synthesis. FloED [15] integrates both optical flow and text prompts, injecting embeddings from both modalities into the inpainting model for object removal. DiffuEraser [25] combines a flow-guided inpainting model with DDIM inversion for improved inpainting fidelity. Senorita-Remover, proposed in [58], introduces instruction-based object removal, using positive prompts to guide removal and negative prompts to suppress unintended object generation in masked areas.

Remark. Compared with previous methods, our **MiniMax-Remover** does not rely on additional prior or prompts. It offers fast inference speed with only 6 sampling steps, no CFG. Despite its simplicity, it achieves a higher object removal success rate and prevent hallucinated object and artifacts generation.

3 Preliminary

Flow Matching. Given an input $\boldsymbol{x} \in \mathbb{R}^{f \times w \times h \times c}$, a pretrained VAE encoder maps it to a latent code $\boldsymbol{z}_0 = \mathcal{E}(\boldsymbol{x}_0) \in \mathbb{R}^{f_1 \times w_1 \times h_1 \times c_1}$. The model input is a noisy latent $\boldsymbol{z}_t$, where $\boldsymbol{z}_t = t\boldsymbol{\epsilon} + (1-t)\boldsymbol{z}_0$, where $\boldsymbol{\epsilon} \sim \mathcal{N}(0, \boldsymbol{I})$ and $t \in [0, 1]$. t is usually sampled from a logit-normal distribution. The target velocity is $\boldsymbol{v} = \boldsymbol{\epsilon} - \boldsymbol{z}_0$. The optimization process of Flow Matching is defined as,

$$\boldsymbol{\theta}^* = \underset{\boldsymbol{\theta}}{\operatorname{argmin}}\, \mathbb{E}_{t, \boldsymbol{z}_t} \left[\| \boldsymbol{u}_{\boldsymbol{\theta}}(\boldsymbol{z}_t, t) - \boldsymbol{v} \|_2^2 \right], \tag{1}$$

$\boldsymbol{u}_{\boldsymbol{\theta}}$ denotes the model parameterized by $\boldsymbol{\theta}$. The model can be a DiT [38] or UNet [43] architecture.

Diffusion-based Video Inpainting. This approach is to reconstruct masked video regions using a conditional diffusion model. The denoising network $\boldsymbol{u}_{\boldsymbol{\theta}}$ takes a noisy latent $\boldsymbol{z}_t$, a masked latent $\boldsymbol{z}_m$, a latent code $\bar{\boldsymbol{m}}$ for the mask $\boldsymbol{m}$, and a condition $\boldsymbol{c}$ as inputs. It optimizes the following objective,

$$\boldsymbol{\theta}^* = \underset{\boldsymbol{\theta}}{\operatorname{argmin}}\, \mathbb{E}_{t, \boldsymbol{z}_t} \left[\| \boldsymbol{u}_{\boldsymbol{\theta}}(\boldsymbol{z}_t, \boldsymbol{z}_m, \bar{\boldsymbol{m}}, \boldsymbol{c}, t) - \boldsymbol{\epsilon}_t \|_2^2 \right]. \tag{2}$$

Generally, $\boldsymbol{c}$ could be optical flow or text prompts.

Classifier-Free Guidance (CFG). CFG [18] improves conditional generation by training the model with and without condition $\boldsymbol{c}$. The network jointly learns the following processes,

$$\boldsymbol{u}_{\boldsymbol{\theta}}(\boldsymbol{z}_t, t, \boldsymbol{c}) \propto -\nabla_{\boldsymbol{z}_t} \log p_{\boldsymbol{\theta}}(\boldsymbol{z}_t | \boldsymbol{c}), \qquad \boldsymbol{u}_{\boldsymbol{\theta}}(\boldsymbol{z}_t, t, \varnothing) \propto -\nabla_{\boldsymbol{z}_t} \log p_{\boldsymbol{\theta}}(\boldsymbol{z}_t), \tag{3}$$

In the inference stage, it combines the following two modes:

$$\hat{\boldsymbol{u}}_{\theta}(\boldsymbol{z}_t, t) = \boldsymbol{u}_{\boldsymbol{\theta}}(\boldsymbol{z}_t, t, \varnothing) + w \cdot (\boldsymbol{u}_{\boldsymbol{\theta}}(\boldsymbol{z}_t, t, \boldsymbol{c}) - \boldsymbol{u}_{\boldsymbol{\theta}}(\boldsymbol{z}_t, t, \varnothing)), \tag{4}$$

where w controls the conditioning strength. However, employing CFG at inference time doubles the computational cost, as it requires two forward passes per sampling step.

MiniMax Optimization. It is widely employed in classical convex optimization [5], robustness enhancement and generative adversarial networks (GANs) [14]. The objective is defined as,

$$\boldsymbol{\theta}^* = \underset{\boldsymbol{\theta}}{\operatorname{argmin}} \max_{\boldsymbol{z}} \mathcal{L}(f(\boldsymbol{z}, \boldsymbol{\theta}), y) \tag{5}$$

where $\mathcal{L}$ is the loss function, f is the model with parameter $\boldsymbol{\theta}$, $\boldsymbol{z}$ and y are the input and ground truth.

4 Methodology

4.1 Overall Framework

As shown in Figure 3, our method can be summarized as two stages.

Stage 1: Training a lightweight video object removal model. Our method follows the standard video inpainting pipeline, but with two simple yet effective improvements. First, we design a lightweight architecture by removing irrelevant components. Unlike many existing methods [59, 55, 48, 25], we do not use text prompts or extra inputs such as optical flow and text prompts, allowing us to remove all cross-attention layers. Second, we introduce two contrastive condition tokens to guide the inpainting process: a *positive token*, which encourages the model to fill in content within the masked regions, and a *negative token*, which discourages the model from generating unwanted objects in those areas. It should be noted that *unlike prior works* [55, 56, 24]*, we only use object mask and do not rely on additional conditions.*

Stage 2: Enhancing model robustness and efficiency via human-guided minimax optimization. We first use the model in Stage 1 to generate inpainted video samples and then ask human annotators to identify successful results. Using this curated subset, we apply a minimax optimization training scheme to enhance the model's robustness and generation quality. Furthermore, the distilled remover can use as few as 6 steps without the help of CFG, resulting a fast inference. The resulting improved model is referred to as **MiniMax-Remover**.

4.2 Stage 1: A Simple Architecture for Video Object Removal

Our method is built on the pretrained video generation model Wan2.1-1.3B [44], which is a Flow Matching model with DiT architecture.

4.2.1 Model Architecture

Input Layer. We start by concatenating three types of latents: a noisy latent $\boldsymbol{z}_t$, a masked latent $\boldsymbol{z}_m$, and a mask latent $\bar{\boldsymbol{m}}$. They are defined as $\boldsymbol{z}_t = t\boldsymbol{\epsilon} + (1-t)\boldsymbol{z}_0$, where $\boldsymbol{z}_0 = \mathcal{E}(\boldsymbol{x})$, $\boldsymbol{z}_m = \mathcal{E}(\boldsymbol{m} \odot \boldsymbol{x})$, and $\bar{\boldsymbol{m}} = \mathcal{E}(\boldsymbol{m})$. Here, $\boldsymbol{x}$ denotes the input video, $t \in [0, 1]$ is the diffusion timestep, and $\mathcal{E}$ is the VAE encoder. Each latent has 16 channels, resulting in a concatenated input of 48 channels. To accommodate this input, we modify the pretrained patch embedding layer to accept 48 channels instead of the original 16. Specifically, the first 16 channels retain the pretrained weights, while the remaining 32 channels are zero-initialized.

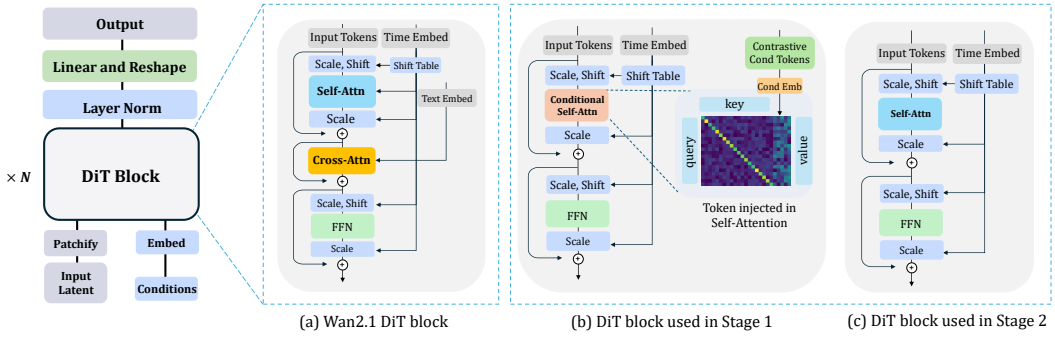

(a) Wan2.1 DiT block (b) DiT block used in Stage 1 (c) DiT block used in Stage 2

Figure 2: The comparison between different blocks. (a) the original Wan2.1 DiT block; (b) DiT block with contrastive tokens (positive or negative token); (c) the block with removing the CFG.

Removing Cross Attention from Pretrained DiT Block. In the pretrained Wan2.1-1.3B [44] model, time information is injected via a *shift table*, a bias-based mechanism to encode timestep information. Additionally, the model employs a cross-attention module to incorporate textual conditioning during video generation. However, for the task of video object removal, textual input is often unnecessary or ambiguous. Therefore, in our model, we remove the textual cross-attention layers in the DiT blocks, while retaining the shift table to preserve time information.

Injecting Contrastive Condition Tokens via Self-Attention. To enable conditional inpainting, we introduce two learnable condition tokens, denoted as $\boldsymbol{c}^+$ (positive token) and $\boldsymbol{c}^-$ (negative token), as a replacement for text embeddings. We refer to these tokens as **contrastive condition tokens**.

Removing the cross-attention from DiT introduces a challenge: how to effectively inject conditional information without relying on textual prompts. A straightforward approach is to repurpose the shift

table to incorporate both timestep and condition information. However, our experiments show that this approach leads to unsatisfactory conditional inpainting results. To achieve more effective conditioning, we instead inject the contrastive condition tokens into the DiT block via the self-attention module. Specifically, we employ a learnable embedding layer to project the conditional token into a high-dimensional feature, and then split the feature into 6 tokens to increase control ability in attention computation process. These condition tokens are concatenated with the original keys and values in the self-attention module, enabling effective conditioning with minimal architectural modifications. For clarity, consider an example: in the original self-attention module, let $\boldsymbol{Q} \in \mathcal{R}^{n\times d}, \boldsymbol{K} \in \mathcal{R}^{n\times d}, \boldsymbol{V} \in \mathcal{R}^{n\times d}$, after injecting the condition tokens, $\boldsymbol{Q} \in \mathcal{R}^{n\times d}, \boldsymbol{K} \in \mathcal{R}^{(n+6)\times d}, \boldsymbol{V} \in \mathcal{R}^{(n+6)\times d}$. The updated DiT block after injecting contrastive condition tokens is illustrated in Figure 2(b).

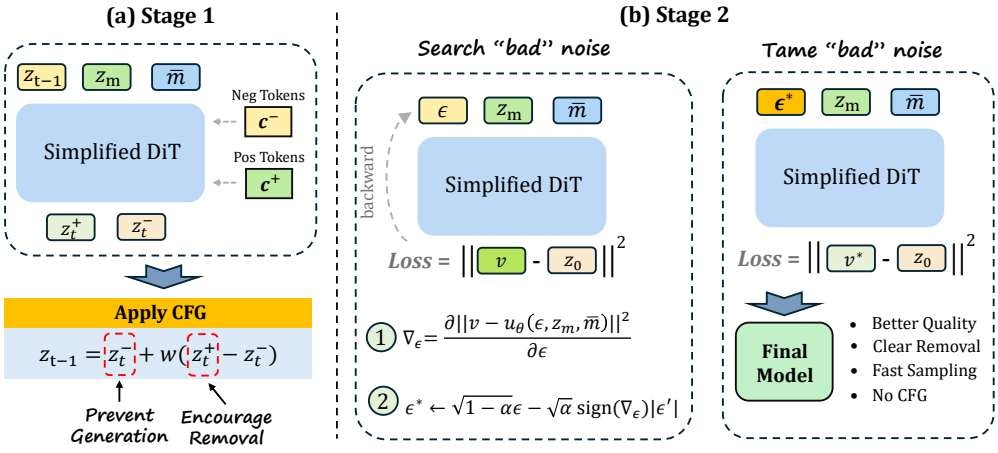

Figure 3: The pipeline of our two-stage method.

4.2.2 Contrastive Conditioning for Object Removal

We employ the positive condition token $\boldsymbol{c}^+$ to guide the remover network in learning object removal and encourage the model to generate target objects under the guidance of $\boldsymbol{c}^-$. Specifically, when applying classifier-free guidance, $\boldsymbol{c}^+$ serves as the positive condition and $\boldsymbol{c}^-$ as the negative condition, steering the model away from regenerating the target objects, preventing the reappearance of undesired objects within the masked regions. To train this behavior, we use two complementary strategies: **First, training the model to remove objects.** We randomly select masks from other videos and apply them to the current original video. The original video is used as the ground truth, and the model is conditioned on the positive prompt $\boldsymbol{c}^+$. Since these masks usually don't match any real object in the current video, the model learns to fill the masked areas using information from the surroundings, instead of trying to recreate an object that fits the mask shape. This helps the model focus on inpainting the background rather than generating new objects. **Second, training the model to generate objects.** We use accurate masks that tightly cover real objects in the same video, along with the negative prompt $\boldsymbol{c}^-$. This teaches the model to connect the shape of the mask with the object it should generate. During inference, we can use $\boldsymbol{c}^-$ as a negative signal to prevent the model from reconstructing the object in those areas. More details are provided in the Appendix.

Given latent features $\boldsymbol{z}_t$, masked latents $\boldsymbol{z}_m$, mask latents $\bar{\boldsymbol{m}}$, and timestep t, the network $\boldsymbol{u}_\theta$ predicts:

$$\hat{\boldsymbol{z}}^+_{t-1} = \boldsymbol{u}_{\boldsymbol{\theta}}(\boldsymbol{z}_t, \boldsymbol{z}_m, \bar{\boldsymbol{m}}, \boldsymbol{c}^+, t), \qquad \hat{\boldsymbol{z}}^-_{t-1} = \boldsymbol{u}_{\boldsymbol{\theta}}(\boldsymbol{z}_t, \boldsymbol{z}_m, \bar{\boldsymbol{m}}, \boldsymbol{c}^-, t). \tag{6}$$

Using CFG with guidance weight w, the final prediction is computed as:

$$\hat{\boldsymbol{z}}_{t-1} = \hat{\boldsymbol{z}}^-_{t-1} + w\big(\hat{\boldsymbol{z}}^+_{t-1} - \hat{\boldsymbol{z}}^-_{t-1}\big). \tag{7}$$

The positive token guides the remover network in learning object removal, and the negative token encourages the model to generate object content. We would like to point out that we employ CFG during Stage 1 of training to facilitate conditional learning. However, CFG is removed in Stage 2 to improve inference efficiency.

4.2.3 Limitations of Stage 1

Despite improvements in simplicity and speed, the current model still faces three limitations. (1) CFG doubles the inference time and requires manual tuning of the guidance scale, which can vary across videos. (2) sampling 50 diffusion steps per frame remains time-consuming. (3) Artifacts or undesired object regeneration may occasionally occur within the intended object removal region, indicating that the contrastive signal is not yet fully effective. To address these limitations, we introduce our Stage 2 method, which is designed to enhance robustness, quality, and efficiency.

4.3 MiniMax-Remover: Distill a Stronger Video Object Remover from Human Feedback

Although our video object remover is trained with contrastive conditioning, it still produces noticeable artifacts and occasionally reconstructs the very object it is supposed to erase. Upon closer examination, we observe that these failure cases are strongly correlated with specific input noise pattens. This insight motivates our objective: to identify such 'bad noise" and train the object removal model to be robust against it.

The minmax optimization also allows us to escape from the CFG usage. In Stage 2, we eliminate CFG to improve sampling efficiency. Specifically, during training, we omit both the positive and the negative condition token. We choose to leave more analysis on this design in Appendix.

Moreover, performing inference with 50 steps is time-consuming. To address this, we distill the model in Stage 1 using the Rectified Flow method [31] to accelerate the sampling process. To build dataset for minimax optimization, we manually selected 10K video pairs from the 17K generated by the Stage 1 model as training data. This not only reduces the number of sampling steps but, with the help of min-max optimization, also encourages the model to produce better object removal results. Consequently, our model formulation changes from $\boldsymbol{u}_{\boldsymbol{\theta}}(\boldsymbol{z}_t, \boldsymbol{z}_m, \bar{\boldsymbol{m}}, \boldsymbol{c}, t)$ to $\boldsymbol{u}_{\boldsymbol{\theta}}(\boldsymbol{z}_t, \boldsymbol{z}_m, \bar{\boldsymbol{m}}, t)$. We formulate our stage-2 training as a minimax optimization problem:

$$\min_{\boldsymbol{\theta}} \max_{\boldsymbol{\epsilon}} \mathbb{E}_t ||\boldsymbol{u}_{\boldsymbol{\theta}}(\boldsymbol{z}_t, \boldsymbol{z}_m, \bar{\boldsymbol{m}}, t) - \boldsymbol{v}||^2, \quad \text{where } \boldsymbol{v} = \boldsymbol{\epsilon} - \boldsymbol{z}_{\text{succ}} \text{ and } \boldsymbol{z}_t = t\boldsymbol{\epsilon} + (1-t)\boldsymbol{z}_0. \tag{8}$$

Therefore, the inner maximization seeks bad noise that maximizes the prediction error, effectively finding challenging input noise. The outer minimization then updates the model parameters $\boldsymbol{\theta}$ to be robust against such adversarial noise. This minimax optimization strategy encourages the model to remain stable even under difficult or misleading input noise.

4.3.1 Search for "Bad" Noise

One of the key challenges in Equation 8 is how to effectively identify a "bad" noise sample $\boldsymbol{\epsilon}$. Rather than directly maximizing the loss in Equation 8 using successful object removal cases, we instead minimize the loss with respect to a bad target: specifically, the original video, which fails to meet the objective of object removal. This leads to the following reformulated objective:

$$\min_{\boldsymbol{\epsilon} \sim \mathcal{N}(0,I)} \left\| \boldsymbol{u}_{\boldsymbol{\theta}}(\boldsymbol{z}_t = \boldsymbol{\epsilon}, \boldsymbol{z}_m, \bar{\boldsymbol{m}}, t = 1.0) - \boldsymbol{v} \right\|^2, \qquad \text{where } \boldsymbol{v} = \text{sg}(\boldsymbol{\epsilon}) - \boldsymbol{z}_{\text{org}}, \tag{9}$$

where $\text{sg}(\cdot)$ is the stop gradient operation and $\boldsymbol{z}_{\text{org}}$ denotes the latent code of the original video. It is important to note that, in Equation 9, we omit the expectation $\mathbb{E}_{t,\boldsymbol{z}_t}$, because we fix the diffusion timestep to $t = 1.0$, making $\boldsymbol{z}_t = \boldsymbol{\epsilon}$.

Starting from a random noise $\boldsymbol{z}_{t=1} = \boldsymbol{\epsilon}$, we compute the gradient of the loss function with respect to $\boldsymbol{\epsilon}$ via backpropagation. This gradient is given by:

$$\nabla_{\boldsymbol{\epsilon}} = \partial \|\boldsymbol{u}_{\boldsymbol{\theta}}(\boldsymbol{\epsilon}, \boldsymbol{z}_m, \bar{\boldsymbol{m}}, t = 1) - \boldsymbol{v}\|^2 / \partial \boldsymbol{\epsilon} \tag{10}$$

After obtaining the gradient with respect to the noise, we can construct a new adversarial ("bad") noise sample $\boldsymbol{\epsilon}^*$ as follows,

$$\boldsymbol{\epsilon}^* \leftarrow \sqrt{1-\alpha}\,\boldsymbol{\epsilon} - \sqrt{\alpha}\ \text{sign}(\nabla_{\boldsymbol{\epsilon}}) \cdot |\boldsymbol{\epsilon}'|, \tag{11}$$

where $\boldsymbol{\epsilon}'$ is a newly sampled noise, $\text{sign}(\nabla_{\boldsymbol{\epsilon}})$ is the sign of the gradient obtained in Equation 10, and $\alpha \in [0, 1]$ is a randomly sampled scalar. We use only the sign of the gradient to suppress the influence of gradient magnitude, ensuring more stable updates. This resulting noise $\boldsymbol{\epsilon}^*$ encodes object-related information that tends to reconstruct the original content, thereby serving as a challenging adversarial noise. Meanwhile, the formulation in Equation 11 preserves the approximate distributional properties of standard Gaussian noise, making $\boldsymbol{\epsilon}^*$ compatible with the diffusion process.

4.3.2 Optimize for Robustness to "Bad" Noise

In Stage 2, we enhance the robustness of the model by fine-tuning it on adversarial noise samples. We minimize the following objective,

$$\min_{\boldsymbol{\theta}} \mathbb{E}_{t,\boldsymbol{z}_t^*} \left\| \boldsymbol{u}_{\boldsymbol{\theta}}(\boldsymbol{z}_t^*, \boldsymbol{z}_m, \bar{\boldsymbol{m}}, t) - \boldsymbol{v}^* \right\|^2, \quad \text{where } \boldsymbol{v}^* = \boldsymbol{\epsilon}^* - \boldsymbol{z}_{\text{succ}} \text{ and } \boldsymbol{z}_t^* = t\boldsymbol{\epsilon}^* + (1-t)\boldsymbol{z}_{\text{succ}}, \quad (12)$$

$\boldsymbol{z}_{\text{succ}}$ is the latent for a successful inpainted video. In Equation 12, we sample a timestep t, and construct a noisy latent input $\boldsymbol{z}_t^*$ according to the previously generated $\boldsymbol{\epsilon}^*$ and $\boldsymbol{z}_{\text{succ}}$. In practice, we train on a mixture of data. Specifically, one-third of training samples are drawn from our curated 10K set with their associated adversarial noises, while the remaining two-thirds are standard WebVid-10M videos with randomly generated object masks. This mixed strategy ensures the model remains effective on both clean and challenging inputs, ultimately leading to improved generalization and resilience against failure cases. We refer to the model after Stage 2 training as MiniMax-Remover.

4.3.3 Advantages of MiniMax-Remover

MiniMax-Remover owns several key advantages:

- **Low Training Overhead**. It only back-propagates once to search the "bad" noise, and trains a remover with simplified architectures which reduces the memory consumption.
- **Fast Inference Speed**. MiniMax-Remover only uses as few as 6 sampling steps without CFG, resulting in significantly faster inference compared to prior methods.
- **High Quality**. Since the model is trained to be robust against "bad" noises, it rarely produces unexpected objects or visual artifacts in the masked regions, resulting in a higher quality.

5 Experiments

Training Dataset. In Stage 1, we use Grounded-SAM2 [29, 42] and captions from CogVLM2 [19] to generate masks on the watermark-free WebVid-10M dataset [1]. Approximately 2.5M video-mask pairs are randomly selected for training. In Stage 2, we collect 17K videos from Pexels [39] and apply the same annotation process as in Stage 1. These are further processed using the model from Stage 1, and 10K videos are manually selected for Stage 2 training.

Training Details. For Stage 1, we initialize our model with Wan2.1-1.3B [44]. Newly added layers, such as the embedding layer, are randomly initialized. The first 16 channels of the patch embedder are copied from Wan2.1, while the remaining 32 are zero-initialized. Training uses a batch size of 128, input frame length of 81, and resolutions randomly sampled from 336×592 to 720×1280. We set the first N mask frames to 0 to support the any-length inpainting by applying sliding windows, using a random ratio of 0.1. We use AdamW optimizer [32] with a constant learning rate of $1e{-}5$, weight decay of $1e{-}4$, and train for 10K steps. In Stage 2, we reuse the model from Stage 1, excluding the embedding layer since no external conditions are needed. One-third of the training iterations apply min-max optimization; the rest follow standard training using unrelated masks from WebVid [1]. Hyperparameters remain the same as in Stage 1. All experiments are conducted on 8 A800 GPUs (80GB each) and take about two days in total.

Inference Details. We perform inference using RTX 4090 GPUs. With an input resolution of 480p and a frame length of 81, ***the inference takes approximately 24 seconds per video*** and consumes around 14GB peak GPU memory(DiT for 8GB, VAE decoding for 6GB), using 6 sampling steps.

Baselines. We compare our method with ProPainter [56], VideoComposer [48], COCOCO [59], FloED [15], DiffuEraser [25], VideoPainter [2] and VACE [21]. We set the evaluate frame length as 32. To evaluate with same frame length, we expand input frame length for VideoComposer [48] and FloED [15]. The rest video inpainters are used their default frame length of their code bases. The frame resolutions are used with their default resolutions.

Metrics. We evaluate background preservation using SSIM and PSNR. TC evaluates the temporal consistency, follows COCOCO [59] and AVID [55] with CLIP-ViT-h-b14 [41] to compute features. GPT-O3 [36] serve as objective metrics. We evaluate these metrics on DAVIS datasets and 200 randomly selected Pexels videos to show generalizations across different datasets. Note that the

200 Pexels videos are not contained in our training datasets, and masks are extracted by Grounded-SAM2. In the user study, participants are presented with a multiple-choice questionnaire to identify which video most effectively removed the target objects from the original video, without introducing blurring, visual artifacts, or hallucinated content within the masked areas.

Table 2: Comparison of different methods on the DAVIS [40] and Pexels [39] datasets. The best results are highlighted in **bold**. "TC" denotes temporal consistency, "VQ" stands for visual quality, and "Succ" represents the success rate.

Method	DAVIS Dataset						Pexels Dataset					
	Quantitative Results			GPT-O3 Eval		User Preference	Quantitative Results			GPT-O3 Eval		User Preference
	SSIM	PSNR	TC	VQ	Succ		SSIM	PSNR	TC	VQ	Succ	
Propainter [56]	0.9748	35.33	0.9769	5.68	56.67	34.55%	0.9746	35.76	0.9813	5.07	35.5	23.28%
VideoComp [48]	0.8689	30.66	0.9529	2.12	7.78	0.25%	0.8865	30.26	0.9573	3.10	14.5	0.245%
COCOCO [59]	0.8863	32.10	0.9511	3.40	12.22	1.96%	0.9145	30.84	0.9693	4.32	30.0	0.245%
FloED [15]	0.9053	32.02	0.9630	5.13	45.56	10.54%	0.9350	34.82	0.9688	4.19	24.5	12.01%
DiffuEraser [25]	0.9818	34.42	0.9767	5.71	56.67	42.40%	0.9859	34.41	0.9800	5.89	59.0	20.83%
VideoPainter [2]	0.9654	34.60	0.9620	3.80	17.98	1.47%	0.9821	36.49	0.9847	5.68	48.0	7.11%
VACE [21]	0.9102	31.92	0.9747	3.12	8.89	2.21%	0.9102	32.33	0.9898	6.27	49.5	23.77%
Ours (6 steps)	0.9842	36.56	0.9770	6.26	82.22	58.08%	0.9873	36.98	0.9905	6.87	76.5	62.01%
Ours (12 steps)	0.9846	36.62	0.9772	6.36	84.44	63.24%	0.9872	**37.02**	**0.9906**	6.86	80.5	**67.15%**
Ours (50 steps)	**0.9847**	**36.66**	**0.9776**	**6.48**	**91.11**	**64.22%**	**0.9878**	36.98	0.9905	**6.90**	**81.0**	63.97%

5.1 Quantitative Comparison

As show in Table 2, our method outperforms previous baselines on all 90 DAVIS videos, achieving an SSIM of 0.9847 and a PSNR of 36.66. Notably, even with only 6 sampling steps, our approach can generate high-quality videos while effectively preserving background details. Furthermore, our method exhibits superior temporal consistency, significantly outperforming generative models such as VACE [21], and even surpassing the traditional inpainting method Propainter [56]. These results demonstrate that our model consistently produces visually pleasing and high-quality video object removal. A similar trend is observed on 200 Pexels videos, where our method achieves the highest SSIM, PSNR, and temporal consistency scores. Moreover, reducing the number of sampling steps does not significantly degrade the removal performance.

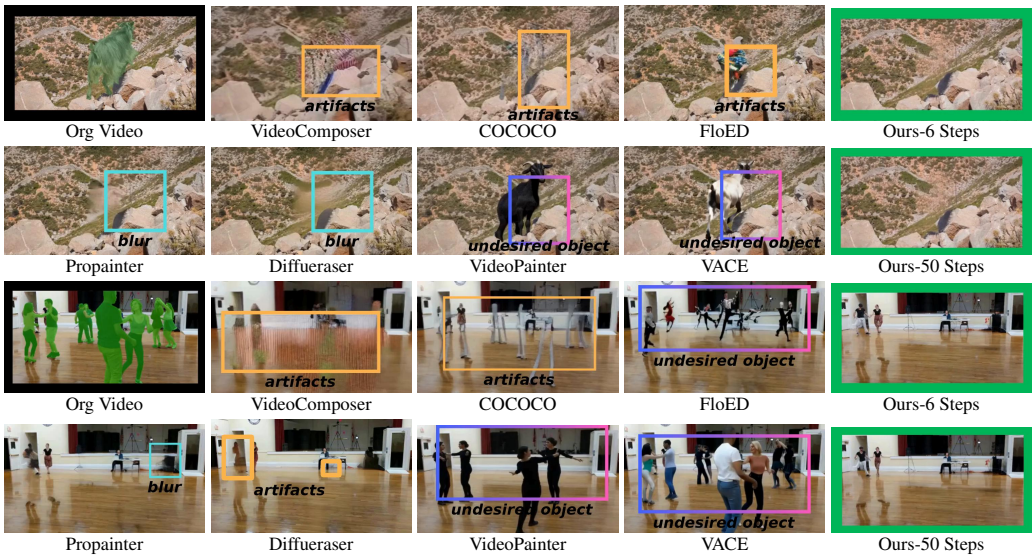

Figure 4: The visual results of our object remover. The video on the left depicts the original video, while the video on the right displays the edited videos. *Best viewed with Acrobat Reader. Click the images to play the animation clips.*

5.2 Qualitative Results

To assess the visual quality and object removal success rate, we utilize GPT-O3 [36], a powerful reasoning large language model, by querying it with evaluation prompts. The quality score ranges from 1 (worst) to 10 (best). According to GPT-O3 evaluation, our method achieves a higher score of 6.48, compared to 5.71 from the best previous method, indicating clearer and more visually appealing removal results. Regarding removal success rate, we prompt the GPT-O3 to determine whether the target objects were effectively removed. Our method achieves a remarkable 91.11% success rate on the DAVIS dataset, far surpassing the previous best of 56.67%. On the Pexels dataset, our method also outperforms previous state-of-the-art approaches, with an 81% success rate compared to 59.0%. Additionally, our method achieves a higher score 6.90, versus 6.27 from prior best methods. For the user preference, it has similar trends, our method achieves the best score on both two datasets compared with previous best remover, 64% vs 42.40% and 67.15% vs 23.77%, respectively.

Table 3: Ablation Study for two stages' training. The best results are **boldfaced**.

Method	Stage	Structure	Condition	•Quantitative Results			•GPT-O3 Evaluation	
				SSIM	PSNR	TC	Visual Quality	Success Rate
Ab-1	Stage 1	ShiftTable+Cross-Attn	Prompt	0.9737	34.77	0.9756	6.27	51.11
Ab-2	Stage 1	ShiftTable+Cross-Attn	Tokens	0.9747	35.09	0.9752	6.37	56.67
Ab-3	Stage 1	ShiftTable	Tokens	0.9682	34.87	0.9743	6.42	53.33
Ab-4	Stage 1	ShiftTable+Self-Attn	Tokens	**0.9798**	**35.87**	**0.9773**	**6.39**	**71.11**
Method	**Stage**	**Data Type**	**Input Noise**	**•Quantitative Results**			**•GPT-O3 Evaluation**	
				SSIM	PSNR	TC	Visual Quality	Success Rate
Ab-1	Stage 2	WebVid Data	Random Noise	0.9781	35.49	0.9759	6.27	65.56
Ab-2	Stage 2	Human Data	Random Noise	0.9796	35.21	0.9772	6.36	72.22
Ab-3	Stage 2	Human Data	Bad Noise-Adv	**0.9847**	**36.66**	**0.9776**	**6.48**	**91.11**

5.3 Ablation Study

To understand the impact of each component and modification in our method, we conduct a step-by-step ablation study. All experiments use 50 sampling steps.

Stage 1. We begin by examining the role of the text encoder and prompt-based conditioning. In the comparison between Ab-1 and Ab-2 (Table 3), we replace the text encoder and prompts with learnable contrastive tokens. The results show no significant drop in performance, indicating that the text encoder is redundant for the removal task when suitable learnable tokens are used instead. Next, comparing Ab-2 and Ab-3, we observe a slight performance degradation after removing the cross-attention module from the DiT. However, when we introduce learnable contrastive condition tokens into the self-attention layers (Ab-4), the results not only recovers but also surpass that of Ab-1. This demonstrates the effectiveness of our simplified DiT architecture.

Stage 2. We compare models trained with and without human-annotated data. The results (Ab-1 vs. Ab-2) show that using manually labeled data alone does not significantly improve performance, likely due to the limited size (10K videos) and diversity of the dataset, which hinders generalization. Furthermore, we compare different noise types used during training (Ab-2 to Ab-3). We find that adding "bad noise" (artificially degraded inputs) into training helps improve performance significantly.

6 Conclusion

In this paper, we propose *MiniMax Remover*, a two-stage framework for object removal in videos. In Stage 1, we simplify the pretrained DiT by removing cross-attention and replacing prompt embeddings with contrastive condition tokens. In Stage 2, we apply min-max optimization: the *max* step searches for challenging noise inputs that lead to failure cases, while the *min* step trains the model to successfully reconstruct the target from these adversarial inputs. Through this two-stage training, our method achieves cleaner and more visually pleasing removal results. Since it requires no classifier-free guidance (CFG) and uses only 6 sampling steps, inference is significantly faster. Extensive experiments demonstrate that our model delivers impressive removal performance across multiple benchmarks.

References

[1] Max Bain, Arsha Nagrani, Gül Varol, and Andrew Zisserman. Frozen in time: A joint video and image encoder for end-to-end retrieval. In *ICCV*, 2021.

[2] Yuxuan Bian, Zhaoyang Zhang, Xuan Ju, Mingdeng Cao, Liangbin Xie, Ying Shan, and Qiang Xu. Videopainter: Any-length video inpainting and editing with plug-and-play context control. In *SIGGRAPH*, 2025.

[3] Black Forest Labs. Black forest labs. `https://github.com/black-forest-labs/flux/`, 2024.

[4] Andreas Blattmann, Robin Rombach, Huan Ling, Tim Dockhorn, Seung Wook Kim, Sanja Fidler, and Karsten Kreis. Align your latents: High-resolution video synthesis with latent diffusion models. In *CVPR*, 2023.

[5] Stephen P Boyd and Lieven Vandenberghe. *Convex optimization*. Cambridge university press, 2004.

[6] Tim Brooks, Aleksander Holynski, and Alexei A Efros. Instructpix2pix: Learning to follow image editing instructions. In *CVPR*, 2023.

[7] Aditya Chandrasekar, Goirik Chakrabarty, Jai Bardhan, Ramya Hebbalaguppe, and Prathosh AP. Remove: A reference-free metric for object erasure. In *CVPRW*, 2024.

[8] Haoxin Chen, Yong Zhang, Xiaodong Cun, Menghan Xia, Xintao Wang, Chao Weng, and Ying Shan. Videocrafter2: Overcoming data limitations for high-quality video diffusion models. In *CVPR*, 2024.

[9] Jiaxin Cheng, Tianjun Xiao, and Tong He. Consistent video-to-video transfer using synthetic dataset. In *ICLR*, 2024.

[10] Yuren Cong, Mengmeng Xu, Christian Simon, Shoufa Chen, Jiawei Ren, Yanping Xie, Juan-Manuel Perez-Rua, Bodo Rosenhahn, Tao Xiang, and Sen He. Flatten: optical flow-guided attention for consistent text-to-video editing. In *ICLR*, 2024.

[11] Gen-3. Introducing gen-3 alpha: A new frontier for video generation. `https://runwayml.com/research/introducing-gen-3-alpha/`, 2024.

[12] Zigang Geng, Binxin Yang, Tiankai Hang, Chen Li, Shuyang Gu, Ting Zhang, Jianmin Bao, Zheng Zhang, Houqiang Li, Han Hu, et al. Instructdiffusion: A generalist modeling interface for vision tasks. In *CVPR*, 2024.

[13] Michal Geyer, Omer Bar-Tal, Shai Bagon, and Tali Dekel. Tokenflow: Consistent diffusion features for consistent video editing. In *ICLR*, 2024.

[14] Ian J Goodfellow, Jean Pouget-Abadie, Mehdi Mirza, Bing Xu, David Warde-Farley, Sherjil Ozair, Aaron Courville, and Yoshua Bengio. Generative adversarial nets. *NeurIPS*, 2014.

[15] Bohai Gu, Hao Luo, Song Guo, and Peiran Dong. Advanced video inpainting using optical flow-guided efficient diffusion. *arXiv:2412.00857*, 2024.

[16] Yuwei Guo, Ceyuan Yang, Anyi Rao, Zhengyang Liang, Yaohui Wang, Yu Qiao, Maneesh Agrawala, Dahua Lin, and Bo Dai. Animatediff: Animate your personalized text-to-image diffusion models without specific tuning. In *ICLR*, 2024.

[17] Yoav HaCohen, Nisan Chiprut, Benny Brazowski, Daniel Shalem, Dudu Moshe, Eitan Richardson, Eran Levin, Guy Shiran, Nir Zabari, Ori Gordon, Poriya Panet, Sapir Weissbuch, Victor Kulikov, Yaki Bitterman, Zeev Melumian, and Ofir Bibi. Ltx-video: Realtime video latent diffusion. *arXiv:2501.00103*, 2024.

[18] Jonathan Ho and Tim Salimans. Classifier-free diffusion guidance. In *NeurIPS Workshop*, 2021.

[19] Wenyi Hong, Weihan Wang, Ming Ding, Wenmeng Yu, Qingsong Lv, Yan Wang, Yean Cheng, Shiyu Huang, Junhui Ji, Zhao Xue, et al. Cogvlm2: Visual language models for image and video understanding. *arXiv:2408.16500*, 2024.

[20] Jiahao Hu, Tianxiong Zhong, Xuebo Wang, Boyuan Jiang, Xingye Tian, Fei Yang, Pengfei Wan, and Di Zhang. Vivid-10m: A dataset and baseline for versatile and interactive video local editing. *arXiv:2411.15260*, 2024.

[21] Zeyinzi Jiang, Zhen Han, Chaojie Mao, Jingfeng Zhang, Yulin Pan, and Yu Liu. Vace: All-in-one video creation and editing. *arXiv:2503.07598*, 2025.

[22] Weijie Kong, Qi Tian, Zijian Zhang, Rox Min, Zuozhuo Dai, Jin Zhou, Jiangfeng Xiong, Xin Li, Bo Wu, Jianwei Zhang, et al. Hunyuanvideo: A systematic framework for large video generative models. *arXiv:2412.03603*, 2024.

[23] Max Ku, Cong Wei, Weiming Ren, Huan Yang, and Wenhu Chen. Anyv2v: A plug-and-play framework for any video-to-video editing tasks. *TMLR*, 2024.

[24] Minhyeok Lee, Suhwan Cho, Chajin Shin, Jungho Lee, Sunghun Yang, and Sangyoun Lee. Video diffusion models are strong video inpainter. In *AAAI*, 2025.

[25] Xiaowen Li, Haolan Xue, Peiran Ren, and Liefeng Bo. Diffueraser: A diffusion model for video inpainting. *arXiv:2501.10018*, 2025.

[26] Chang Liu, Rui Li, Kaidong Zhang, Yunwei Lan, and Dong Liu. Stablev2v: Stablizing shape consistency in video-to-video editing. *arXiv:2411.11045*, 2024.

[27] Shaoteng Liu, Tianyu Wang, Jui-Hsien Wang, Qing Liu, Zhifei Zhang, Joon-Young Lee, Yijun Li, Bei Yu, Zhe Lin, Soo Ye Kim, et al. Generative video propagation. In *CVPR*, 2025.

[28] Shaoteng Liu, Yuechen Zhang, Wenbo Li, Zhe Lin, and Jiaya Jia. Video-p2p: Video editing with cross-attention control. In *CVPR*, 2024.

[29] Shilong Liu, Zhaoyang Zeng, Tianhe Ren, Feng Li, Hao Zhang, Jie Yang, Chunyuan Li, Jianwei Yang, Hang Su, Jun Zhu, and Lei Zhang. Grounding dino: Marrying dino with grounded pre-training for open-set object detection. In *ECCV*, 2024.

[30] Shiyu Liu, Yucheng Han, Peng Xing, Fukun Yin, Rui Wang, Wei Cheng, Jiaqi Liao, Yingming Wang, Honghao Fu, Chunrui Han, Guopeng Li, Yuang Peng, Quan Sun, Jingwei Wu, Yan Cai, Zheng Ge, Ranchen Ming, Lei Xia, Xianfang Zeng, Yibo Zhu, Binxing Jiao, Xiangyu Zhang, Gang Yu, and Daxin Jiang. Step1x-edit: A practical framework for general image editing. *arXiv:2504.17761*, 2025.

[31] Xingchao Liu, Chengyue Gong, and Qiang Liu. Flow straight and fast: Learning to generate and transfer data with rectified flow. *arXiv:2209.03003*, 2022.

[32] Ilya Loshchilov and Frank Hutter. Decoupled weight decay regularization. In *ICLR*, 2019.

[33] Guoqing Ma, Haoyang Huang, Kun Yan, Liangyu Chen, Nan Duan, Shengming Yin, Changyi Wan, Ranchen Ming, Xiaoniu Song, Xing Chen, et al. Step-video-t2v technical report: The practice, challenges, and future of video foundation model. *arXiv:2502.10248*, 2025.

[34] Mochi-1. Mochi-1. `https://www.genmo.ai/blog`, 2024.

[35] Chong Mou, Mingdeng Cao, Xintao Wang, Zhaoyang Zhang, Ying Shan, and Jian Zhang. Revideo: Remake a video with motion and content control. In *NeurIPS*, 2024.

[36] Introducing OpenAI o3 and o4 mini. https://openai.com/index/introducing-o3-and-o4-mini/, 2025.

[37] OpenAI. Sora: Creating video from text. `https://openai.com/index/sora/`, 2024.

[38] William Peebles and Saining Xie. Scalable diffusion models with transformers. In *ICCV*, 2023.

[39] Pexels. https://www.pexels.com/, 2024.

[40] Jordi Pont-Tuset, Federico Perazzi, Sergi Caelles, Pablo Arbeláez, Alex Sorkine-Hornung, and Luc Van Gool. The 2017 davis challenge on video object segmentation. In *CVPRW*, 2017.

[41] Aditya Ramesh, Mikhail Pavlov, Gabriel Goh, Scott Gray, Chelsea Voss, Alec Radford, Mark Chen, and Ilya Sutskever. Zero-shot text-to-image generation. In *ICML*, 2021.

[42] Nikhila Ravi, Valentin Gabeur, Yuan-Ting Hu, Ronghang Hu, Chaitanya Ryali, Tengyu Ma, Haitham Khedr, Roman Rädle, Chloe Rolland, Laura Gustafson, Eric Mintun, Junting Pan, Kalyan Vasudev Alwala, Nicolas Carion, Chao-Yuan Wu, Ross Girshick, Piotr Dollár, and Christoph Feichtenhofer. Sam 2: Segment anything in images and videos. In *ICLR*, 2025.

[43] Olaf Ronneberger, Philipp Fischer, and Thomas Brox. U-net: Convolutional networks for biomedical image segmentation. In *MICCAI*, 2015.

[44] Ang Wang, Baole Ai, Bin Wen, Chaojie Mao, Chen-Wei Xie, Di Chen, Feiwu Yu, Haiming Zhao, Jianxiao Yang, Jianyuan Zeng, Jiayu Wang, Jingfeng Zhang, Jingren Zhou, Jinkai Wang, Jixuan Chen, Kai Zhu, Kang Zhao, Keyu Yan, Lianghua Huang, Mengyang Feng, Ningyi Zhang, Pandeng Li, Pingyu Wu, Ruihang Chu, Ruili Feng, Shiwei Zhang, Siyang Sun, Tao Fang, Tianxing Wang, Tianyi Gui, Tingyu Weng, Tong Shen, Wei Lin, Wei Wang, Wei Wang, Wenmeng Zhou, Wente Wang, Wenting Shen, Wenyuan Yu, Xianzhong Shi, Xiaoming Huang, Xin Xu, Yan Kou, Yangyu Lv, Yifei Li, Yijing Liu, Yiming Wang, Yingya Zhang, Yitong Huang, Yong Li, You Wu, Yu Liu, Yulin Pan, Yun Zheng, Yuntao Hong, Yupeng Shi, Yutong Feng, Zeyinzi Jiang, Zhen Han, Zhi-Fan Wu, and Ziyu Liu. Wan: Open and advanced large-scale video generative models. *arXiv:2503.20314*, 2025.

[45] Fu-Yun Wang, Zhaoyang Huang, Alexander Bergman, Dazhong Shen, Peng Gao, Michael Lingelbach, Keqiang Sun, Weikang Bian, Guanglu Song, Yu Liu, et al. Phased consistency models. *NeurIPS*, 2024.

[46] Jiuniu Wang, Hangjie Yuan, Dayou Chen, Yingya Zhang, Xiang Wang, and Shiwei Zhang. Modelscope text-to-video technical report. 2023.

[47] Su Wang, Chitwan Saharia, Ceslee Montgomery, Jordi Pont-Tuset, Shai Noy, Stefano Pellegrini, Yasumasa Onoe, Sarah Laszlo, David J Fleet, Radu Soricut, et al. Imagen editor and editbench: Advancing and evaluating text-guided image inpainting. In *CVPR*, 2023.

[48] Xiang Wang, Hangjie Yuan, Shiwei Zhang, Dayou Chen, Jiuniu Wang, Yingya Zhang, Yujun Shen, Deli Zhao, and Jingren Zhou. Videocomposer: Compositional video synthesis with motion controllability. *NeurIPS*, 2023.

[49] Jay Zhangjie Wu, Yixiao Ge, Xintao Wang, Stan Weixian Lei, Yuchao Gu, Yufei Shi, Wynne Hsu, Ying Shan, Xiaohu Qie, and Mike Zheng Shou. Tune-a-video: One-shot tuning of image diffusion models for text-to-video generation. In *ICCV*, 2023.

[50] Shiyuan Yang, Zheng Gu, Liang Hou, Xin Tao, Pengfei Wan, Xiaodong Chen, and Jing Liao. Mtv-inpaint: Multi-task long video inpainting. *arXiv:2503.11412*, 2025.

[51] Zhuoyi Yang, Jiayan Teng, Wendi Zheng, Ming Ding, Shiyu Huang, Jiazheng Xu, Yuanming Yang, Wenyi Hong, Xiaohan Zhang, Guanyu Feng, Da Yin, Xiaotao Gu, Yuxuan Zhang, Weihan Wang, Yean Cheng, Ting Liu, Bin Xu, Yuxiao Dong, and Jie Tang. Cogvideox: Text-to-video diffusion models with an expert transformer. In *ICLR*, 2025.

[52] Kai Zhang, Lingbo Mo, Wenhu Chen, Huan Sun, and Yu Su. Magicbrush: A manually annotated dataset for instruction-guided image editing. *NeurIPS*, 2023.

[53] Lvmin Zhang and Maneesh Agrawala. Packing input frame context in next-frame prediction models for video generation. *arXiv:2504.12626*, 2025.

[54] Lvmin Zhang, Anyi Rao, and Maneesh Agrawala. Adding conditional control to text-to-image diffusion models. In *ICCV*, 2023.

[55] Zhixing Zhang, Bichen Wu, Xiaoyan Wang, Yaqiao Luo, Luxin Zhang, Yinan Zhao, Peter Vajda, Dimitris Metaxas, and Licheng Yu. Avid: Any-length video inpainting with diffusion model. *arXiv:2312.03816*, 2023.

[56] Shangchen Zhou, Chongyi Li, Kelvin CK Chan, and Chen Change Loy. Propainter: Improving propagation and transformer for video inpainting. In *ICCV*, 2023.

[57] Junhao Zhuang, Yanhong Zeng, Wenran Liu, Chun Yuan, and Kai Chen. A task is worth one word: Learning with task prompts for high-quality versatile image inpainting. In *ECCV*, 2024.

[58] Bojia Zi, Penghui Ruan, Marco Chen, Xianbiao Qi, Shaozhe Hao, Shihao Zhao, Youze Huang, Bin Liang, Rong Xiao, and Kam-Fai Wong. Senorita-2m: A high-quality instruction-based dataset for general video editing by video specialists. *arXiv:2502.06734*, 2025.

[59] Bojia Zi, Shihao Zhao, Xianbiao Qi, Jianan Wang, Yukai Shi, Qianyu Chen, Bin Liang, Kam-Fai Wong, and Lei Zhang. Cococo: Improving text-guided video inpainting for better consistency, controllability and compatibility. In *AAAI*, 2025.

NeurIPS Paper Checklist

1. **Claims**

   Question: Do the main claims made in the abstract and introduction accurately reflect the paper's contributions and scope?

   Answer: [Yes]

   Justification: We have made the main claims in the abstract and introduction.

   Guidelines:

   - The answer NA means that the abstract and introduction do not include the claims made in the paper.
   - The abstract and/or introduction should clearly state the claims made, including the contributions made in the paper and important assumptions and limitations. A No or NA answer to this question will not be perceived well by the reviewers.
   - The claims made should match theoretical and experimental results, and reflect how much the results can be expected to generalize to other settings.
   - It is fine to include aspirational goals as motivation as long as it is clear that these goals are not attained by the paper.

2. **Limitations**

   Question: Does the paper discuss the limitations of the work performed by the authors?

   Answer: [Yes]

   Justification: We have discussed the limitation in Appendix.

   Guidelines:

   - The answer NA means that the paper has no limitation while the answer No means that the paper has limitations, but those are not discussed in the paper.
   - The authors are encouraged to create a separate "Limitations" section in their paper.
   - The paper should point out any strong assumptions and how robust the results are to violations of these assumptions (e.g., independence assumptions, noiseless settings, model well-specification, asymptotic approximations only holding locally). The authors should reflect on how these assumptions might be violated in practice and what the implications would be.
   - The authors should reflect on the scope of the claims made, e.g., if the approach was only tested on a few datasets or with a few runs. In general, empirical results often depend on implicit assumptions, which should be articulated.
   - The authors should reflect on the factors that influence the performance of the approach. For example, a facial recognition algorithm may perform poorly when image resolution is low or images are taken in low lighting. Or a speech-to-text system might not be used reliably to provide closed captions for online lectures because it fails to handle technical jargon.
   - The authors should discuss the computational efficiency of the proposed algorithms and how they scale with dataset size.
   - If applicable, the authors should discuss possible limitations of their approach to address problems of privacy and fairness.
   - While the authors might fear that complete honesty about limitations might be used by reviewers as grounds for rejection, a worse outcome might be that reviewers discover limitations that aren't acknowledged in the paper. The authors should use their best judgment and recognize that individual actions in favor of transparency play an important role in developing norms that preserve the integrity of the community. Reviewers will be specifically instructed to not penalize honesty concerning limitations.

3. **Theory assumptions and proofs**

   Question: For each theoretical result, does the paper provide the full set of assumptions and a complete (and correct) proof?

   Answer: [NA]

   Justification: We do not include any theoretical result.

   Guidelines:

- The answer NA means that the paper does not include theoretical results.
- All the theorems, formulas, and proofs in the paper should be numbered and cross-referenced.
- All assumptions should be clearly stated or referenced in the statement of any theorems.
- The proofs can either appear in the main paper or the supplemental material, but if they appear in the supplemental material, the authors are encouraged to provide a short proof sketch to provide intuition.
- Inversely, any informal proof provided in the core of the paper should be complemented by formal proofs provided in appendix or supplemental material.
- Theorems and Lemmas that the proof relies upon should be properly referenced.

4. **Experimental result reproducibility**

   Question: Does the paper fully disclose all the information needed to reproduce the main experimental results of the paper to the extent that it affects the main claims and/or conclusions of the paper (regardless of whether the code and data are provided or not)?

   Answer: [Yes]

   Justification: We have provided all necessary information to enable the reproduction of the paper's Sec 4.

   Guidelines:

   - The answer NA means that the paper does not include experiments.
   - If the paper includes experiments, a No answer to this question will not be perceived well by the reviewers: Making the paper reproducible is important, regardless of whether the code and data are provided or not.
   - If the contribution is a dataset and/or model, the authors should describe the steps taken to make their results reproducible or verifiable.
   - Depending on the contribution, reproducibility can be accomplished in various ways. For example, if the contribution is a novel architecture, describing the architecture fully might suffice, or if the contribution is a specific model and empirical evaluation, it may be necessary to either make it possible for others to replicate the model with the same dataset, or provide access to the model. In general. releasing code and data is often one good way to accomplish this, but reproducibility can also be provided via detailed instructions for how to replicate the results, access to a hosted model (e.g., in the case of a large language model), releasing of a model checkpoint, or other means that are appropriate to the research performed.
   - While NeurIPS does not require releasing code, the conference does require all submissions to provide some reasonable avenue for reproducibility, which may depend on the nature of the contribution. For example
     (a) If the contribution is primarily a new algorithm, the paper should make it clear how to reproduce that algorithm.
     (b) If the contribution is primarily a new model architecture, the paper should describe the architecture clearly and fully.
     (c) If the contribution is a new model (e.g., a large language model), then there should either be a way to access this model for reproducing the results or a way to reproduce the model (e.g., with an open-source dataset or instructions for how to construct the dataset).
     (d) We recognize that reproducibility may be tricky in some cases, in which case authors are welcome to describe the particular way they provide for reproducibility. In the case of closed-source models, it may be that access to the model is limited in some way (e.g., to registered users), but it should be possible for other researchers to have some path to reproducing or verifying the results.

5. **Open access to data and code**

   Question: Does the paper provide open access to the data and code, with sufficient instructions to faithfully reproduce the main experimental results, as described in supplemental material?

   Answer: [Yes]

   Justification: We have written these details in Sec 4.

   Guidelines:

   - The answer NA means that paper does not include experiments requiring code.

- Please see the NeurIPS code and data submission guidelines (`https://nips.cc/public/guides/CodeSubmissionPolicy`) for more details.
- While we encourage the release of code and data, we understand that this might not be possible, so "No" is an acceptable answer. Papers cannot be rejected simply for not including code, unless this is central to the contribution (e.g., for a new open-source benchmark).
- The instructions should contain the exact command and environment needed to run to reproduce the results. See the NeurIPS code and data submission guidelines (`https://nips.cc/public/guides/CodeSubmissionPolicy`) for more details.
- The authors should provide instructions on data access and preparation, including how to access the raw data, preprocessed data, intermediate data, and generated data, etc.
- The authors should provide scripts to reproduce all experimental results for the new proposed method and baselines. If only a subset of experiments are reproducible, they should state which ones are omitted from the script and why.
- At submission time, to preserve anonymity, the authors should release anonymized versions (if applicable).
- Providing as much information as possible in supplemental material (appended to the paper) is recommended, but including URLs to data and code is permitted.

6. **Experimental setting/details**

   Question: Does the paper specify all the training and test details (e.g., data splits, hyperparameters, how they were chosen, type of optimizer, etc.) necessary to understand the results?

   Answer: [Yes]

   Justification: We have described these details in the Sec 4.

   Guidelines:

   - The answer NA means that the paper does not include experiments.
   - The experimental setting should be presented in the core of the paper to a level of detail that is necessary to appreciate the results and make sense of them.
   - The full details can be provided either with the code, in appendix, or as supplemental material.

7. **Experiment statistical significance**

   Question: Does the paper report error bars. suitably and correctly defined or other appropriate information about the statistical significance of the experiments?

   Answer: [No]

   Justification: We don't report these information.

   Guidelines:

   - The answer NA means that the paper does not include experiments.
   - The authors should answer "Yes" if the results are accompanied by error bars, confidence intervals, or statistical significance tests, at least for the experiments that support the main claims of the paper.
   - The factors of variability that the error bars are capturing should be clearly stated (for example, train/test split, initialization, random drawing of some parameter, or overall run with given experimental conditions).
   - The method for calculating the error bars should be explained (closed form formula, call to a library function, bootstrap, etc.)
   - The assumptions made should be given (e.g., Normally distributed errors).
   - It should be clear whether the error bar is the standard deviation or the standard error of the mean.
   - It is OK to report 1-sigma error bars, but one should state it. The authors should preferably report a 2-sigma error bar than state that they have a 96% CI, if the hypothesis of Normality of errors is not verified.
   - For asymmetric distributions, the authors should be careful not to show in tables or figures symmetric error bars that would yield results that are out of range (e.g. negative error rates).
   - If error bars are reported in tables or plots, The authors should explain in the text how they were calculated and reference the corresponding figures or tables in the text.

8. **Experiments compute resources**

   Question: For each experiment, does the paper provide sufficient information on the computer resources (type of compute workers, memory, time of execution) needed to reproduce the experiments?

   Answer: [Yes]

   Justification: We have provided the details of computer resources in Sec 4.

   Guidelines:

   - The answer NA means that the paper does not include experiments.
   - The paper should indicate the type of compute workers CPU or GPU, internal cluster, or cloud provider, including relevant memory and storage.
   - The paper should provide the amount of compute required for each of the individual experimental runs as well as estimate the total compute.
   - The paper should disclose whether the full research project required more compute than the experiments reported in the paper (e.g., preliminary or failed experiments that didn't make it into the paper).

9. **Code of ethics**

   Question: Does the research conducted in the paper conform, in every respect, with the NeurIPS Code of Ethics `https://neurips.cc/public/EthicsGuidelines`?

   Answer: [Yes]

   Guidelines:

   - The answer NA means that the authors have not reviewed the NeurIPS Code of Ethics.
   - If the authors answer No, they should explain the special circumstances that require a deviation from the Code of Ethics.
   - The authors should make sure to preserve anonymity (e.g., if there is a special consideration due to laws or regulations in their jurisdiction).

10. **Broader impacts**

    Question: Does the paper discuss both potential positive societal impacts and negative societal impacts of the work performed?

    Answer: [Yes]

    Justification: We put these information in Appendix.

    Guidelines:

    - The answer NA means that there is no societal impact of the work performed.
    - If the authors answer NA or No, they should explain why their work has no societal impact or why the paper does not address societal impact.
    - Examples of negative societal impacts include potential malicious or unintended uses (e.g., disinformation, generating fake profiles, surveillance), fairness considerations (e.g., deployment of technologies that could make decisions that unfairly impact specific groups), privacy considerations, and security considerations.
    - The conference expects that many papers will be foundational research and not tied to particular applications, let alone deployments. However, if there is a direct path to any negative applications, the authors should point it out. For example, it is legitimate to point out that an improvement in the quality of generative models could be used to generate deepfakes for disinformation. On the other hand, it is not needed to point out that a generic algorithm for optimizing neural networks could enable people to train models that generate Deepfakes faster.
    - The authors should consider possible harms that could arise when the technology is being used as intended and functioning correctly, harms that could arise when the technology is being used as intended but gives incorrect results, and harms following from (intentional or unintentional) misuse of the technology.
    - If there are negative societal impacts, the authors could also discuss possible mitigation strategies (e.g., gated release of models, providing defenses in addition to attacks, mechanisms for monitoring misuse, mechanisms to monitor how a system learns from feedback over time, improving the efficiency and accessibility of ML).

11. **Safeguards**

    Question: Does the paper describe safeguards that have been put in place for responsible release of data or models that have a high risk for misuse (e.g., pretrained language models, image generators, or scraped datasets)?

    Answer: [Yes]

    Justification: These details are included in the Appendix.

    Guidelines:

    - The answer NA means that the paper poses no such risks.
    - Released models that have a high risk for misuse or dual-use should be released with necessary safeguards to allow for controlled use of the model, for example by requiring that users adhere to usage guidelines or restrictions to access the model or implementing safety filters.
    - Datasets that have been scraped from the Internet could pose safety risks. The authors should describe how they avoided releasing unsafe images.
    - We recognize that providing effective safeguards is challenging, and many papers do not require this, but we encourage authors to take this into account and make a best faith effort.

12. **Licenses for existing assets**

    Question: Are the creators or original owners of assets (e.g., code, data, models), used in the paper, properly credited and are the license and terms of use explicitly mentioned and properly respected?

    Answer: [Yes]

    Justification: All creators and original owners are properly credited. All license and terms of use explicitly mentioned and properly respected.

    Guidelines:

    - The answer NA means that the paper does not use existing assets.
    - The authors should cite the original paper that produced the code package or dataset.
    - The authors should state which version of the asset is used and, if possible, include a URL.
    - The name of the license (e.g., CC-BY 4.0) should be included for each asset.
    - For scraped data from a particular source (e.g., website), the copyright and terms of service of that source should be provided.
    - If assets are released, the license, copyright information, and terms of use in the package should be provided. For popular datasets, `paperswithcode.com/datasets` has curated licenses for some datasets. Their licensing guide can help determine the license of a dataset.
    - For existing datasets that are re-packaged, both the original license and the license of the derived asset (if it has changed) should be provided.
    - If this information is not available online, the authors are encouraged to reach out to the asset's creators.

13. **New assets**

    Question: Are new assets introduced in the paper well documented and is the documentation provided alongside the assets?

    Answer: [NA]

    Justification: Our paper doesn't release new assets.

    Guidelines:

    - The answer NA means that the paper does not release new assets.
    - Researchers should communicate the details of the dataset/code/model as part of their submissions via structured templates. This includes details about training, license, limitations, etc.
    - The paper should discuss whether and how consent was obtained from people whose asset is used.
    - At submission time, remember to anonymize your assets (if applicable). You can either create an anonymized URL or include an anonymized zip file.

14. **Crowdsourcing and research with human subjects**

Question: For crowdsourcing experiments and research with human subjects, does the paper include the full text of instructions given to participants and screenshots, if applicable, as well as details about compensation (if any)?

Answer: [No]

Justification: We haven't put these information in our paper.

Guidelines:

- The answer NA means that the paper does not involve crowdsourcing nor research with human subjects.
- Including this information in the supplemental material is fine, but if the main contribution of the paper involves human subjects, then as much detail as possible should be included in the main paper.
- According to the NeurIPS Code of Ethics, workers involved in data collection, curation, or other labor should be paid at least the minimum wage in the country of the data collector.

15. **Institutional review board (IRB) approvals or equivalent for research with human subjects**

Question: Does the paper describe potential risks incurred by study participants, whether such risks were disclosed to the subjects, and whether Institutional Review Board (IRB) approvals (or an equivalent approval/review based on the requirements of your country or institution) were obtained?

Answer: [Yes]

Justification: We told them before sending them questionnaire.

Guidelines:

- The answer NA means that the paper does not involve crowdsourcing nor research with human subjects.
- Depending on the country in which research is conducted, IRB approval (or equivalent) may be required for any human subjects research. If you obtained IRB approval, you should clearly state this in the paper.
- We recognize that the procedures for this may vary significantly between institutions and locations, and we expect authors to adhere to the NeurIPS Code of Ethics and the guidelines for their institution.
- For initial submissions, do not include any information that would break anonymity (if applicable), such as the institution conducting the review.

16. **Declaration of LLM usage**

Question: Does the paper describe the usage of LLMs if it is an important, original, or non-standard component of the core methods in this research? Note that if the LLM is used only for writing, editing, or formatting purposes and does not impact the core methodology, scientific rigorousness, or originality of the research, declaration is not required.

Answer: [NA]

Justification: Core method development in this research does not involve LLMs as any important, original, or non-standard components.

Guidelines:

- The answer NA means that the core method development in this research does not involve LLMs as any important, original, or non-standard components.
- Please refer to our LLM policy (`https://neurips.cc/Conferences/2025/LLM`) for what should or should not be described.

7 More Details of Stage-1 Training

Here, we provide further details on the training process of Stage 1. We adopt the same mask selection strategy as in Senorita-Remover [58]. In this paper, we propose to simplify the pretrained DiT architecture and replace the prompts with learnable contrastive condition tokens.

The most challenging issue in object removal is the undesired regeneration problem, where the model tends to regenerate objects in the masked region that share a similar shape to the mask itself. To address this issue, as illustrated in Figure 5, we introduce contrastive condition tokens: a positive token c^+ to guide the model towards object removal, and a negative token c^- to guide object generation within the masked region. This allows the model to leverage CFG for effective object removal while preventing the reappearance of similar objects in the masked areas.

In Figure 5(a), when selecting masks, we randomly select masks from other unrelated videos, and paste the masks into the input video. These masks are designed to differ in shape from the actual objects within the masked region of the input video. As a result, the model, trained on such data, tends to generate content that differs from the mask shape during inference. This process is considered as the positive condition c^+. The position condition learns to remove the masked objects.

In Figure 5(b), we incorporate training samples using their corresponding precise masks. In these cases, the masked region contains an object whose shape closely matches the mask. Training on such data encourages the model to regenerate similar objects in the masked region when conditioned on c^-. This contrastive training strategy helps the model distinguish between removal and generation tasks more effectively. This process is considered as the negative condition c^-. The negative condition learns to generate the masked objects.

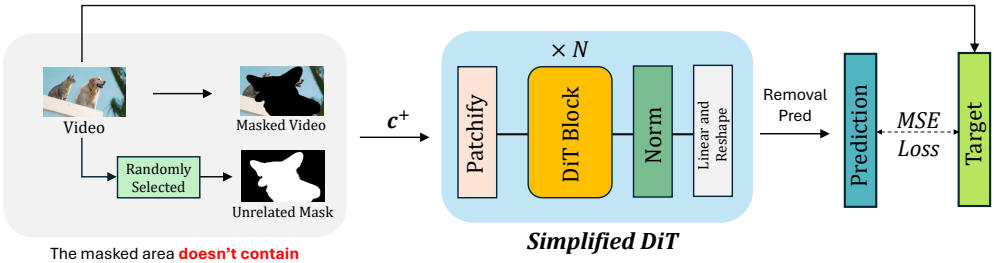

(a) Learn Removal

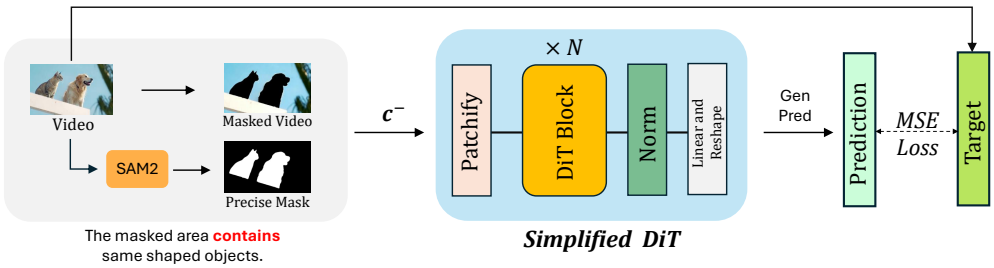

(b) Learn Generation

Figure 5: Training framework of the Stage-1. (a) denotes the positive condition process, and the position condition learns to remove the masked objects. and (b) represents the negative process, and the negative condition learns to generate the masked objects..

8 Explanation Of Why CFG Can Be Discarded

8.1 MiniMax Optimization

In our work, we formulate the min-max remover using the following objective:

$$\min_{\boldsymbol{\theta}} \max_{\boldsymbol{\epsilon}^*} \left\| \boldsymbol{u}_{\boldsymbol{\theta}}(\boldsymbol{\epsilon}^*, \boldsymbol{z}_m, \bar{\boldsymbol{m}}) - \boldsymbol{z}^* \right\|^2, \tag{13}$$

where $\boldsymbol{u}$ is a DiT network parameterized by $\boldsymbol{\theta}$, and $\boldsymbol{v}^* = \boldsymbol{\epsilon}^* - \boldsymbol{z}_{\text{succ}}$, with $\boldsymbol{z}_{\text{succ}} = \mathcal{E}(\boldsymbol{x}_{\text{succ}})$. Here, $\boldsymbol{x}_{\text{succ}}$ is a video clip filtered and accepted by human annotators, and $\mathcal{E}$ is the autoencoder.

In practice, to search for the "bad" noise, we replace the inner maximization with:

$$\min_{\boldsymbol{\epsilon}^*} \left\| \boldsymbol{u}_{\boldsymbol{\theta}}(\boldsymbol{\epsilon}^*, \boldsymbol{z}_{\boldsymbol{m}}, \bar{\boldsymbol{m}}) - \boldsymbol{v}^* \right\|^2, \tag{14}$$

where $\boldsymbol{v}^* = \boldsymbol{\epsilon}^* - \boldsymbol{z}_{\text{org}}$, and $\boldsymbol{z}_{\text{org}}$ corresponds to an undesired generation. This approach finds a noise $\boldsymbol{\epsilon}^*$ that causes $\boldsymbol{u}_{\boldsymbol{\theta}}$ to fail. By subsequently training $\boldsymbol{\theta}$ to minimize the objective even under such challenging noise, the model learns to produce outputs that deviate from the poor generation target $\boldsymbol{v}^*$.

8.2 Minimax Optimization Encourages Correct Removal and Discourages "Bad" Removal

Minimax Optimization Encourages Correct Removal. Based on the principles of minimax optimization discussed above, we have that:

$$||\boldsymbol{u}_{\boldsymbol{\theta}}(\boldsymbol{\epsilon}, \boldsymbol{z}_m, \bar{\boldsymbol{m}}) - (\boldsymbol{\epsilon} - \boldsymbol{z}_{\text{succ}})||^2 \leq ||\boldsymbol{u}_{\boldsymbol{\theta}}(\boldsymbol{\epsilon}^*, \boldsymbol{z}_{\boldsymbol{m}}, \bar{\boldsymbol{m}}) - (\boldsymbol{\epsilon}^* - \boldsymbol{z}_{\text{succ}})||^2. \tag{15}$$

This inequality implies that minimizing the loss on the "bad" input noise $\boldsymbol{\epsilon}^*$ leads to improved performance on the clean input noise $\boldsymbol{\epsilon}$. Consequently, the model is incentivized to generate outputs that increasingly align with desired removals.

Minimax Optimization Discourages "Bad" Removals. As shown in the formulation,

$$\min_{\boldsymbol{\theta}} \left\| \boldsymbol{u}_{\boldsymbol{\theta}}(\boldsymbol{\epsilon}^*, \boldsymbol{z}_{\boldsymbol{m}}, \bar{\boldsymbol{m}}) - (\boldsymbol{\epsilon}^* - \boldsymbol{z}_{\text{succ}}) \right\|^2,$$

the model is optimized to ensure that, upon convergence, no "bad" input noise $\boldsymbol{\epsilon}^*$ can lead to a failure-inducing removal. Consequently, the model inherently avoids generating such "bad" removals.

In summary, this min-max training strategy enables the model to avoid producing poor outputs (aligned with the Stage 1 negative condition c^-) while encouraging alignment with high-quality generations (aligned with the Stage 1 positive condition c^+). Therefore, after the minimax optimization, we can discard the classifier-free guidance (CFG), and the quality of removal results remains unaffected.

Experiments. Here, we conduct experiments to demonstrate that discarding CFG does not significantly affect performance. To ensure a fair comparison, we use the human-annotated data from Stage 2 and reuse the Stage 1 model without removing the tokens injected into the self-attention layer. Thus, the ablation variant *ab-1* applies CFG by introducing two learnable contrastive tokens, c^+ and c^-. The sampling process consists of 50 steps, while all other training and inference settings remain consistent with those described in the main text. As shown in Table 4, using CFG leads to a slight improvement in background preservation and temporal consistency, but results in marginal decreases in visual quality and success rate. These results further support that the model performs robustly even without CFG.

Table 4: Comparison of results with/without CFG on the DAVIS [40] dataset. TC indicates Temporal Consistency, while Succ Rate stands for Success Rate. The best results are **boldfaced**.

Method	•Quantitative Results			•GPT-O3 Evaluation	
	SSIM	PSNR	TC	Quality	Succ Rate
MiniMax-Remover(w CFG)	**0.9853**	**36.76**	**0.9778**	6.45	90.00
MiniMax-Remover(w/o CFG)	0.9847	36.66	0.9776	**6.48**	**91.11**

9 Why Use Adversarial-Based Noise?

9.1 Comparison of Adversarial-Based Noise with Other Types of Noise

It might seem intuitive to replace adversarial-based noise with either random or inversion-based noise. However, our experiments clearly justify the use of adversarial noise.

Table 5: Ablation study on different noise types using the DAVIS dataset [40]. TC denotes Temporal Consistency, and Succ Rate indicates Success Rate. The best results are highlighted in **bold**.

Method	Input Noise	•Quantitative Metrics			•GPT-O3 Evaluation	
		SSIM	PSNR	TC	Quality	Succ Rate
Ablation Study-1	Random Noise	0.9796	35.21	0.9772	6.36	72.22
Ablation Study-2	Inversion-Based Noise	0.9797	35.80	0.9768	5.81	70.00
Ablation Study-3 (Ours)	Adversarial-Based Noise	**0.9847**	**36.66**	**0.9776**	**6.48**	**91.11**

Random noise fails to guide the model towards adversarial directions. As a result, when training on limited data for a large number of iterations, it often leads to overfitting without improving model robustness or performance.

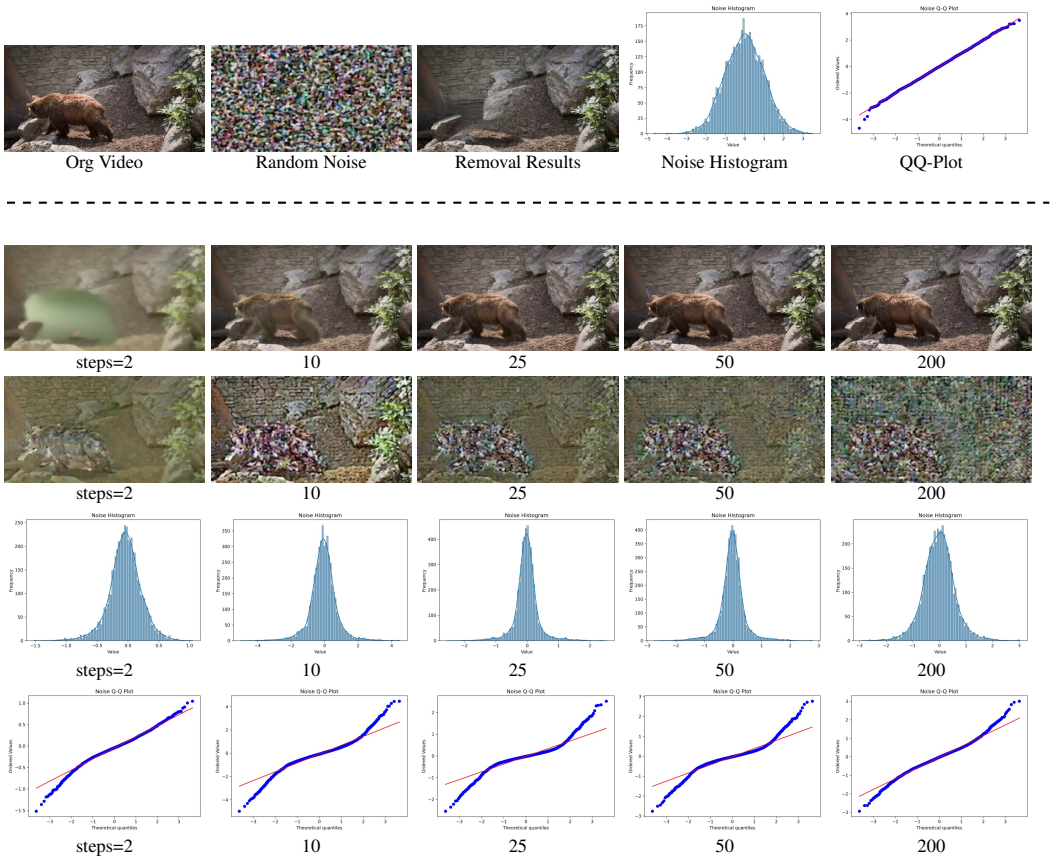

Figure 6: Visual results of the Stage-1 Object Remover under inversion-based noises. The top row presents the original video, random noise, removal results, the corresponding histogram, and QQ plot. Rows 2 to 5 at the bottom display the removal results with inversion-based noise, the inversion-based noise itself, and its associated histogram and QQ plot, respectively. *Best viewed with Acrobat Reader. Click the images to play the animation clips.*

Inversion-based noise, on the other hand, typically requires many optimization steps to reconstruct noise from latent representations. To keep the computational cost comparable to adversarial noise, we restrict this process to just three steps. However, such shallow inversion retains a significant amount of information from the latents, violating the assumption that noise follows a standard Gaussian distribution $\mathcal{N}(\mathbf{0}, \boldsymbol{I})$. Consequently, it cannot be considered "random" noise in a true sense.

In contrast, **adversarial noise** is constructed by updating the input noise in a direction that maximizes model failure, while still keeping it within the $\mathcal{N}(\mathbf{0}, \boldsymbol{I})$ distribution. Specifically, we apply the update

rule:

$$\boldsymbol{\epsilon}^* \leftarrow \sqrt{1-\alpha}\,\boldsymbol{\epsilon} - \sqrt{\alpha} \cdot \text{sign}(\nabla_{\boldsymbol{\epsilon}}) \cdot |\boldsymbol{\epsilon}'|$$

This allows us to craft noise that remains statistically valid but strategically challenging for the model.

As shown in Table 5, adversarial-based noise significantly outperforms both random and inversion-based noise across all evaluation metrics, demonstrating its effectiveness in improving model robustness and generalization.

9.2 Determining Whether the Noise is Gaussian

To assess whether the noise follows a Gaussian distribution, we typically use visual tools such as histograms and QQ-plots. The histogram provides an overview of the noise distribution, while the QQ-plot compares the quantiles of the observed noise with those of a standard Gaussian distribution. If the points in the QQ-plot lie approximately along a straight line, this suggests that the noise is likely Gaussian.

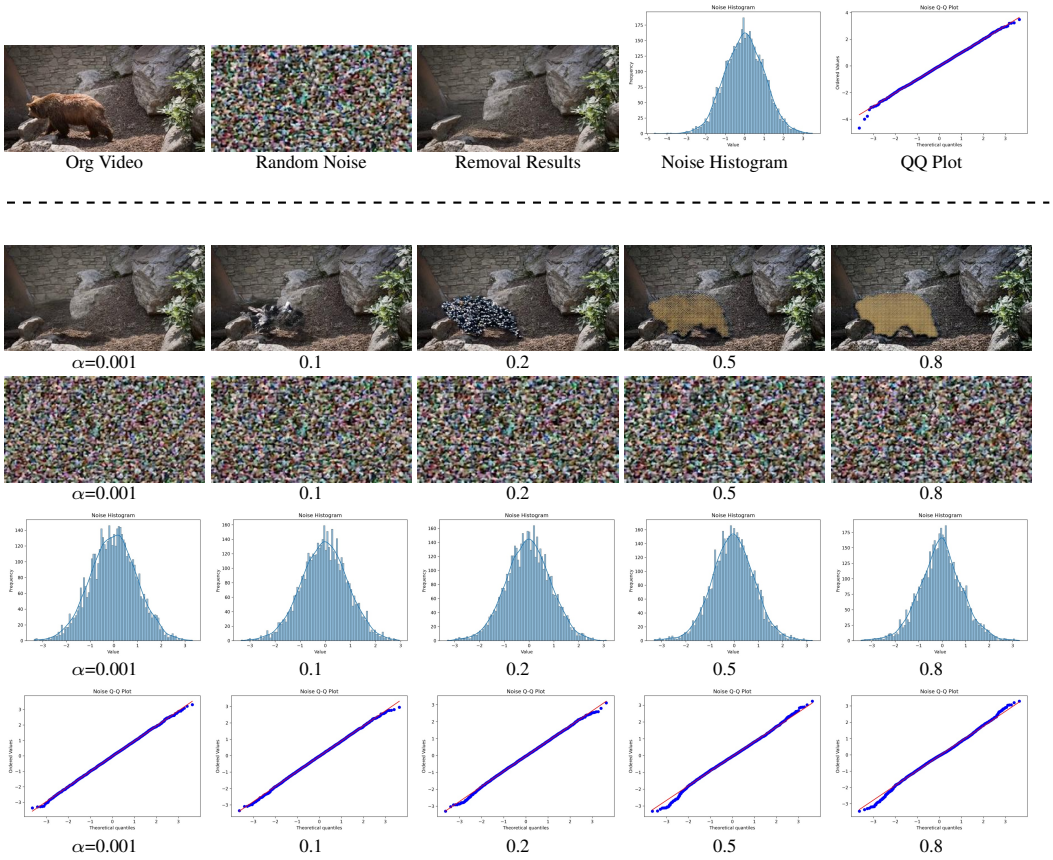

Figure 7: Visual results of the Stage-1 Object Remover under adversarial-based noises. The top row illustrates the original video, random noise input, the resulting object removal output, along with the corresponding noise histogram and QQ plot. The lower section comprises the object removal results under adversarial-based noise (second row), the visualization of the adversarial noise (third row), and its associated histogram and QQ plot (fourth row). *Best viewed with Acrobat Reader. Click the images to play the animation clips.*

Inversion-Based Noise is Non-Gaussian. As shown in Figure 6, both the histogram and QQ-plot reveal a clear deviation from the characteristics of Gaussian noise. Inversion-based noise exhibits a distribution that significantly differs from that of random noise. These visualizations support the conclusion that inversion-based noise does not follow a Gaussian distribution and is therefore unsuitable for training purposes. Moreover, the visualizations suggest that inversion-based noise retains information from the original latent representations, further compromising its utility as pure

noise. In addition, generating such noise requires multiple iterations of the inversion process, making it computationally expensive and impractical for large-scale applications.

Adversarial-Based Noise Approximates a Gaussian Distribution. Figure 7 presents the histogram and QQ-plot for adversarial-based noise. The visual evidence indicates that this type of noise closely approximates a Gaussian distribution. The visualizations also suggest that the noise is random and does not retain any information from the original latent representations. Both the histogram and QQ-plot are highly similar to those of standard Gaussian random noise. As a result, adversarial-based noise not only effectively perturbs model predictions but also serves as a suitable and reliable noise source for training. Notably, it can be generated efficiently using a single step of backpropagation.

Figure 8: Visual Results of the Minimax-Remover with Adversarial-Based Noise. Adversarial-based noise is integrated into the Minimax-Remover, yielding visually robust and consistent removal performance. *Best viewed with Acrobat Reader. Click the images to play the animation clips.*

9.3 Testing Adversarial-Based Noise on the Robust MiniMax-Remover

We assess the performance of the robust Minimax-Remover when subjected to adversarial-based noise. Specifically, we apply adversarial noise to Minimax-Remover and gradually increase the noise level α from 0.001 to 0.8. As illustrated in Figure 8, our method successfully removes objects from video frames effectively, maintaining high visual quality when $\alpha < 0.5$. Even as the noise level increases beyond 0.5, the removal results may become slightly blurred, but no regenerated objects or visual artifacts are observed. This demonstrates that the MiniMax-Remover is resilient to high levels of adversarial-based noise and can still produce clean and reliable removal results under challenging conditions.

10 The Prompt used for GPT-O3 Evaluation

The evaluation is conducted using the `GPT-O3-2025-04-16` model. We employ the following prompt to assess visual quality and success rate.

Prompt for Quality Evaluation

Human: Please evaluate the visual quality of the object-removal result in this image pair: the left panel shows the original frame with the target object highlighted by a blue mask, and the right panel shows the frame after the object has been removed. Rate the quality of the removal on a scale from 1 to 10, where 10 means a seamless, high-resolution result with no visible artifacts, 5 indicates some noise or artifacts but overall acceptable quality, and 1 corresponds to an unacceptable, very poor result. Return only the numeric score.

<Image> Image 1</Image>
<Image> Image 2</Image>
...
GPT-O3: ...

Prompt for Success Rate Evaluation

Human: This is a video object removal task. The object to be removed is already marked in blue in the image on the left. Please determine whether the object has been successfully removed. A successful removal is defined by the following criteria:

1. The object has been completely removed.
2. There is no visible blurriness in the removal area (not background blur, but unnatural foreground blur that is inconsistent with the surrounding context).
3. There are no moiré patterns or artifacts in the region (e.g., unnatural textures that differ significantly from human visual expectations).
4. No new, unwanted objects have been generated in the area (e.g., the tiger is removed but a bear appears instead, or another tiger is generated).
5. Shadows not in the masked region are considered successfully removed.

Think it step by step. Then provide a final judgment by answering with "yes" or "no"

<Image> Image 1</Image>
<Image> Image 2</Image>

...
GPT-O3: ...

11 More Experimental Results

11.1 Evaluation of ReMOVE Metrics

Table 6: Comparison on the ReMOVE benchmark (higher is better).

Method	ReMOVE (w/o Crop)	ReMOVE (w/ Crop)
ProPainter [56]	0.8634	0.9259
FloED [15]	0.6950	0.8103
DiffuEraser [25]	0.8621	0.9212
COCOCO [59]	0.8009	0.8994
VideoComposer [48]	0.6605	0.7429
VideoPainter [2]	0.6955	0.8279
VACE [21]	0.5731	0.7723
MiniMax-Remover (6 steps)	0.8831	0.9401
MiniMax-Remover (12 steps)	0.8843	0.9405
MiniMax-Remover (50 steps)	**0.8850**	**0.9416**

Table 6 reports quantitative comparisons on the ReMOVE benchmark [7], a reference-free metric for evaluating object removal quality (higher is better). Our method consistently achieves the best performance under both ReMOVE (w/o Crop) and ReMOVE (w/ Crop) settings. Specifically, our 50-step model attains scores of 0.8850 and 0.9416, outperforming the strongest baseline ProPainter by +0.0216 and +0.0157, respectively. These results demonstrate the superior removal fidelity and spatial consistency of our approach.

Across all methods, the w/ Crop results are higher than the w/o Crop results, indicating that localized evaluation around the target region is generally easier. Nevertheless, our model maintains the highest accuracy in both configurations, highlighting its robustness to complex backgrounds and global contextual variations.

Overall, our model demonstrates strong generalization and stability across different evaluation conditions, surpassing prior state-of-the-art methods such as ProPainter [56], DiffuEraser [25], and COCOCO [59] on both global and localized ReMOVE metrics.

11.2 Can GPT-O3 be trusted?

Table 7: Consistency with human annotations on 100 removal samples.

Assessment Type	GPT-4O	GPT-4O-mini	GPT-4-turbo	GPT-O3
Acc in Failure Cases	94.0%	98.0%	86.0%	**96.0%**
Acc in Success Cases	88.0%	26.0%	58.0%	**94.0%**
Overall Accuracy	91.0%	62.0%	72.0%	**95.0%**

Table 8: Consistency with human annotations on 100 multi-object videos.

Assessment Type	GPT-4O	GPT-4O-mini	GPT-4-turbo	GPT-O3
Acc in Failure Cases	90.0%	92.0%	86.0%	**98.0%**
Acc in Success Cases	**90.0%**	48.0%	48.0%	86.0%
Overall Accuracy	90.0%	70.0%	67.0%	**92.0%**

We evaluate four models on two datasets with balanced splits of successes and failures and use masks to highlight the removed regions for evaluation. As reported in Table 7, GPT-O3 attains 96.0% accuracy in failure cases and 94.0% in success cases for 95.0% overall, GPT-4O records 94.0% and 88.0% for 91.0% overall, GPT-4-turbo reaches 86.0% and 58.0% for 72.0% overall, and GPT-4O-mini achieves 98.0% and 26.0% for 62.0% overall. Table 8 summarizes the 100 multi object video removals where GPT-O3 again leads with 98.0% in failure cases and 86.0% in success cases for 92.0% overall, while GPT-4O achieves 90.0% in both overall and success accuracy and GPT-4-turbo and GPT-4O-mini reach 67.0% and 70.0% overall respectively. Together Tables 7 and 8 show that GPT-O3 aligns best with human annotations by balancing recognition of failures and true successes.

11.3 Results on Multi-Object Videos

We evaluate on a multi-mask subset of DAVIS to stress multi-object editing and report SSIM, PSNR, Temporal Consistency, Visual Quality, and Success Rate in Table 9. MiniMax-Remover achieves the best overall results, with the 50-step variant reaching SSIM 0.9847, PSNR 36.69, TC 0.9780, VQ 6.70, and Succ 92.59%. This clearly outperforms strong baselines such as ProPainter at SSIM 0.9778 and PSNR 35.64 and DiffuEraser at SSIM 0.9769 and PSNR 35.08, while also yielding much higher VQ and task success. Traditional inpainting methods show reasonable pixel metrics but struggle in complex multi-mask interactions, which leads to lower VQ and Succ, as seen with VideoComposer at VQ 2.13 and Succ 9.26%. Performance scales with sampling steps for our method: 6 to 12 steps provides a notable gain, and 12 to 50 steps offers smaller but consistent improvements that help on hard cases. Overall, MiniMax-Remover balances temporal stability and detail restoration most effectively on DAVIS multi-mask videos.

11.4 Results on Dynamic Background Videos

As shown in Table 10, our method consistently achieves the best results among all methods on the DAVIS dynamic background subset. The 50-step version reaches the highest SSIM of 0.9828, PSNR of 36.48, and success rate of 91.36, showing clear superiority in both reconstruction and perceptual quality. Traditional methods such as ProPainter and DiffuEraser fall behind in success rate and VQ. Increasing steps improves MiniMax-Remover steadily, confirming the robustness of iterative refinement. Overall, MiniMax-Remover maintains strong temporal consistency while significantly enhancing visual fidelity and task success compared with prior baselines.

Table 9: Comparison of methods on multi-objects videos. TC denotes Temporal Consistency, VQ denotes Visual Quality, and Succ denotes Success Rate.

Method	SSIM	PSNR	TC	VQ	Succ
ProPainter [56]	0.9778	35.64	0.9773	5.67	57.41
VideoComposer [48]	0.8967	31.14	0.9546	2.13	9.26
COCOCO [59]	0.9101	32.98	0.9523	3.37	11.11
FLoED [15]	0.8887	32.72	0.9691	5.09	42.59
DiffuEraser [25]	0.9769	35.08	0.9790	5.81	57.41
VideoPainter [2]	0.9652	35.17	0.9634	5.00	24.44
VACE [21]	0.8949	32.67	0.9732	3.20	5.56
MiniMax-Remover (6 steps)	0.9842	36.62	0.9773	6.41	85.18
MiniMax-Remover (12 steps)	0.9843	36.64	0.9778	6.31	87.04
MiniMax-Remover (50 steps)	**0.9847**	**36.69**	**0.9780**	**6.70**	**92.59**

Table 10: Comparison of different methods on dynamic background videos. TC denotes Temporal Consistency, VQ denotes Visual Quality, and Succ denotes Success Rate.

Method	SSIM	PSNR	TC	VQ	Succ
ProPainter [56]	0.9781	35.78	0.9778	5.53	53.09
COCOCO [59]	0.9125	33.26	0.9546	3.29	12.35
FLoED	0.8892	32.75	0.9663	5.07	43.21
DiffuEraser [25]	0.9741	35.12	0.9778	5.68	55.56
VideoComposer [48]	0.8936	31.31	0.9531	2.13	8.64
VideoPainter [2]	0.9652	35.49	0.9623	3.88	19.75
VACE [21]	0.8942	32.72	0.9762	2.97	7.41
MiniMax-Remover (6 steps)	0.9821	36.42	0.9786	6.16	81.48
MiniMax-Remover (12 steps)	0.9823	36.46	0.9787	6.23	86.42
MiniMax-Remover (50 steps)	**0.9828**	**36.48**	**0.9789**	**6.46**	**91.36**

Table 11: Effect of dilation size on MiniMax-Remover. TC denotes Temporal Consistency, VQ denotes Visual Quality, and Succ denotes Success Rate.

Dilation	SSIM	PSNR	TC	VQ	Succ
2	0.9830	36.49	0.9764	6.37	91.11
6	**0.9847**	**36.66**	0.9776	**6.48**	91.11
12	0.9838	36.38	0.9778	6.40	**92.22**
24	0.9829	36.36	**0.9789**	6.33	84.44

11.5 Tightness/looseness of the mask

As shown in the Table 11, moderate dilation values yield the best balance between structure and temporal smoothness. Dilation 6 achieves the highest SSIM of 0.9847 and PSNR of 36.66 with strong visual quality, while dilation 12 gives the best success rate of 92.22. Very small or large dilation slightly reduce performance, indicating that moderate spatial context improves reconstruction and temporal consistency.

11.6 The Implementation of Learnable Contrastive Tokens

```python
import torch
import torch.nn as nn

class TokenEmbedding(nn.Module):
    def __init__(self, dim):
        super().__init__()
        self.dim = dim
        # The first token represents the C+
        # The second token represents the C-.
        self.token_embedding = nn.Embedding(2, dim)
        # using 6 tokens to enhance contrastive tokens.
        self.mlp = nn.Linear(dim, 6 * dim)
        self.act_fn = nn.SiLU()

    def forward(self, input_ids):
        bsz = input_ids.size(0)
        x = self.act_fn(self.token_embedding(input_ids))
        x = self.mlp(x).view(bsz, -1, 6, self.dim)
        return x

class Stage1_Model(nn.Module):
    def __init__(self, config):
        super().__init__()
        ...
        self.token_embed = TokenEmbedding(dim)
        ...

    def forward(self, hidden_states, input_ids):
        ...
        tokens = self.token_embed(input_ids)
        l = hidden_states.shape[1]
        hidden_states = torch.cat([hidden_states, tokens], dim=1)
        ...
        hidden_states = self.attn(query, key, value)[:,:l]
        ...
        return hidden_states
```

Pseudo Codes for Stage-1 Model.

11.7 The Impact of Learnable Token Number

Table 12: Comparison of different token configurations in stage-1. TC denotes Temporal Consistency, VQ denotes Visual Quality, and Succ denotes Success Rate.

Method	Tokens	SSIM	PSNR	TC	VQ	Succ
stage-1	1	0.9778	35.82	0.9774	6.13	66.67
stage-1	2	**0.9801**	**35.88**	**0.9776**	6.23	70.00
stage-1	6	0.9798	35.87	0.9773	6.39	**71.11**
stage-1	8	0.9792	35.85	0.9772	**6.46**	**71.11**

As shown in Table 12, using six tokens achieves the best trade-off across all metrics. While the two-token setting slightly improves SSIM and PSNR, the six-token model attains the highest VQ score (6.39) and the best success rate (71.11 %), indicating superior overall quality and stability. Increasing to eight tokens yields no further gain and even reduces SSIM and PSNR, suggesting over-fragmentation. Therefore, the six-token configuration provides the optimal balance between reconstruction fidelity and perceptual consistency.

12 Broader Impacts

Minimax-Remover is a diffusion-based model for removing objects from videos in only 6 inference steps without CFG. It enables efficient video editing, film post-production by simplifying complex visual manipulation. However, like all generative models, it could be misused to create deceptive or fake videos, potentially causing misinformation or reputational harm. To mitigate such risks, we will release the model under a CC BY-NC 4.0 license, restricting commercial use and large-scale deployment.

13 Limitation and Future Work

In this study, we present a fast and effective method for video object removal that does not rely on CFG. However, our approach has some limitations. First, the object remover in Stage 2 was trained using only 10,000 videos. Second, while the DiT model is efficient, a large portion of the computational overhead comes from the VAE encoding and decoding processes. In future work, we plan to expand the dataset to enhance the remover's robustness and explore the use of a smaller VAE to speed up inference.